INFORMATION TO USERS

This reproduction was made from a copy of a document sent to us for microfilming. While the most advanced technology has been used to photograph and reproduce this document, the quality of the reproduction is heavily dependent upon the quality of the material submitted.

The following explanation of techniques is provided to help clarify markings or notations which may appear on this reproduction.

1. The sign or "target" for pages apparently lacking from the document photographed is "Missing Page(s)". If it was possible to obtain the missing page(s) or section, they are spliced into the film along with adjacent pages. This may have necessitated cutting through an image and duplicating adjacent pages to assure complete continuity.

2. When an image on the film is obliterated with a round black mark, it is an indication of either blurred copy because of movement during exposure, duplicate copy, or copyrighted materials that should not have been filmed. For blurred pages, a good image of the page can be found in the adjacent frame. If copyrighted materials were deleted, a target note will appear listing the pages in the adjacent frame.

3. When a map, drawing or chart, etc., is part of the material being photographed, a definite method of "sectioning" the material has been followed. It is customary to begin filming at the upper left hand corner of a large sheet and to continue from left to right in equal sections with small overlaps. If necessary, sectioning is continued again - beginning below the first row and continuing on until complete.

4. For illustrations that cannot be satisfactorily reproduced by xerographic means, photographic prints can be purchased at additional cost and inserted into your xerographic copy. These prints are available upon request from the Dissertations Customer Services Department.

5. Some pages in any document may have indistinct print. In all cases the best available copy has been filmed.

University Microfilms International
300 N. Zeeb Road
Ann Arbor, MI 48106

Order Number 1334151

Fundamental studies on electrochemical production of Al-Li alloys from oxyfluoride melts

Narayan, Ananth Ramchandran, M.S.

University of Nevada, Reno, 1988

U·M·I
300 N. Zeeb Rd.
Ann Arbor, MI 48106

PLEASE NOTE:

In all cases this material has been filmed in the best possible way from the available copy. Problems encountered with this document have been identified here with a check mark __✓__.

1. Glossy photographs or pages _____
2. Colored illustrations, paper or print _____
3. Photographs with dark background _____
4. Illustrations are poor copy _____
5. Pages with black marks, not original copy _____
6. Print shows through as there is text on both sides of page _____
7. Indistinct, broken or small print on several pages _____
8. Print exceeds margin requirements _____
9. Tightly bound copy with print lost in spine _____
10. Computer printout pages with indistinct print _____
11. Page(s) _____ lacking when material received, and not available from school or author.
12. Page(s) _____ seem to be missing in numbering only as text follows.
13. Two pages numbered _____. Text follows.
14. Curling and wrinkled pages _____
15. Dissertation contains pages with print at a slant, filmed as received ✓
16. Other _____

_____

_____

University of Nevada-Reno

FUNDAMENTAL STUDIES ON ELECTROCHEMICAL PRODUCTION OF Al-Li ALLOYS FROM OXYFLUORIDE MELTS

A thesis submitted in partial fulfillment
of the requirements for the degree of
Master of Science
in
Metallurgical Engineering

by

Ananth R. Narayan

January 1988

The thesis of Ananth R. Narayan is approved :

Thesis Advisor

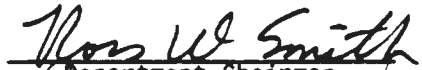

Department Chairman

Dean, Graduate School

University of Nevada
Reno

January 1988

ACKNOWLEDGEMENTS

The author thanks Dr. R.G.Reddy (thesis advisor) for his constant supervision and encouragement in the course of this project as well as to Dr. D.A. Jones and Dr. D. Noble for their criticism and advice. The author is indebted to Mr. E. Morrice for his help in setting up the experimental apparatus. Grateful acknowledgement is made to Mackay Minerals Resources Research Institute and Research Advisory Board, University of Nevada-Reno, for the financial support.

CONTENTS

LIST OF TABLES

LIST OF FIGURES

ABSTRACT

A new process for the direct production of Aluminum lithium alloys in fluoride melts using low cost lithium oxide as a lithium source was investigated. Lithium was electrolytically deposited from $4LiF.CaF_2$ $+Li_2O$(sat.) electrolyte using a graphite anode and liquid aluminum cathode. From the point of extraction of metals from oxides in fluoride melts, the solubility of the oxide in the fluoride melt is important since it is the dissolved oxide which reacts with the electrodes to form the metal. The solubility of Li_2O was found to increase from 10.6 wt.% at 1058K to 14.8 wt.% at 1133K and this was sufficient to attempt further experimental investigations on the electrolysis process. The overvoltage on the graphite anode was measured as a function of applied current density to obtain a deeper insight into the reaction mechanisms at the anode. A two electron charge transfer reaction at the anode in the Tafel region and a limiting current density phenomenon above 0.37 A/cm^2 was observed. The oxyfluoride complex species was predicted to be predominantly $LiOF^{2-}$. The effect of temperature and electrolyte composition on the cell efficiency was studied. An optimum temperature of 1121K with $4LiF.CaF_2+Li_2O$(sat.) electrolyte showed the highest cathode current efficiency. The cathode current efficiency increased with increasing wt.% of LiF in the electrolyte and an optimum value of 36% was obtained for the cathode current efficiency at 1130K. The liquidus temperature of the electrolyte decides the process temperature and attempts to reduce the liquidus temperature by the addition of

fluoride compounds would improve the efficiency of the cell. This would also reduce the redissolution of lithium in the electrolyte.

1. Introduction

The use of light-weight aluminum lithium alloy air-frame structures in civil and military aircraft are projected to increase from 15 pct. in 1990 to 33 pct. by 1995 (1). The increase in demand was due to 1) rapid escalation of fuel costs 2) higher thrust for more fuel efficient aircraft and 3) improved structural properties for Al-Li alloys over the existing Al alloys. Reduction in aircraft weight is one means of decreasing fuel consumption. Because aluminum alloys comprise 80 weight percent of this airframe, development of low-density structural aluminum alloys have been of significant interest. Lithium improves both modulus and density when alloyed with aluminum. Each weight percent lithium added to an alloy reduces the density 3 percent and increases the elastic modulus by 6 percent (2). Recent studies show that addition of lithium to aluminum also improves the corrosion resistance (3). The present commercial method for production of aluminum-lithium alloys is by powder metallurgy or melting and casting methods involving the use of pure metallic lithium, the latter being added to the molten aluminum (1). Production of aluminum-lithium alloys by mixing the pure metals is an energy intensive and expensive process. The relatively high prices for high-purity lithium metal is an important factor in the cost of producing Al-Li alloys. To avoid the necessity of preparing high-purity lithium, a new process has been investigated to prepare aluminum lithium alloys by in-situ electrolysis of lithium oxide in fluoride electrolytes.

Presently, all lithium metal is produced by electrolysis of lithium fluoride and aluminum lithium alloys are produced by the mixing of constituent melts (1). It requires approximately 6 pounds of LiCl to make one pound of lithium metal (4) and at present the world production of the metal is about 500 tons.The current pricing of lithium is $18.50 per pound (5) depending on sodium content. The high price of the metal is due to the concentration of the element in the raw material, the energy required to liberate the element and the sales volume.

The principle objective of the described research is to develop physico-chemical information that can be applied to the direct production of aluminum-lithium alloys for use in the manufacture of high-strength, low-density structures. Specifically, the following fundamental information was determined by experimental investigation: 1) The solubility of Li_2O in $LiF-CaF_2$ electrolyte as a function of temperature. The solubility of Li_2O in the fluoride melt must be significant because it is only the dissolved oxide in the complex oxyfluoride form which is available for reduction at the anode during electrolysis. 2) The anodic overvoltage on graphite during electrolysis of fluoride electrolyte plus lithium oxide melts. Anode reaction mechanism was determined and the nature of the complex oxyfluoride species was predicted.3) Efficiency of electrolysis was determined as a function of temperature and composition of electrolyte.

2. PREVIOUS WORK

2.1 Solubility of Oxides in Halide Melts

To study the viability of a process for obtaining a metal from its oxide, it is necessary to obtain sufficient information on the solubility characteristics of the oxide in the fluoride melt. While extensive studies have been done for Al_2O_3-cryolite systems(6-9), very little work has been done for other oxide-halide systems .

Belyayaev (10) found that mixed fluorides, particularly cryolite, (Na_3AlF_6) are good solvents for metal oxides while Stern (11) found that molten chlorides have a very limited solubility for metal oxides. Haupin (12) studied the solubility of Al_2O_3 in $AlCl_3$-LiCl melts and predicted a simple model for the reaction between the oxide and chloride to form the dissolved species. He predicted the dissolved species to be AlOCl and found that the Al_2O_3 solubility increases with the cube root of activity of $AlCl_3$. Wai and Blander (13) studied the solubility of Al_2O_3 in eutectic LiCl-KCl containing dissolved $AlCl_3$ using a proton activation technique. The presence of AlO^+ complex species in the melt was identified and a formation constant for the AlO^+ complex was deduced. From the solubility data, they obtained a value of 300KJ/mole for the specific bond free energy for the Al^{3+} and O^{2-} ions.

Suito and Gaskell (14) measured depression of freezing points of MgF_2, BaF_2 and CaF_2 due to addition of different oxides. Activities of several oxides in fluorides as a function of liquidus composition was calculated. They found that the results obtained with infrared

absorption technique are in good agreement with their proposed theoretical model. The solubility of rare earth oxides in cryolite-alumina based melts were investigated (15). Regression equations for the dissolution of La_2O_3, CeO_2 and Y_2O_3 as a function of temperature and cryolite alumina ratio were obtained. The solubility of above oxides studied increased with increasing temperature and with decreasing cryolite-alumina ratio. Collected data on solubility of several oxide fluoride systems are tabulated in Table 1. From the table it is observed that the solubility of rare earth oxides in fluoride melts is in the range of 2 to 3 weight % and a minimum of 2 wt. % solubility of lithium oxide is required for the process to be feasible.

2.2 Production of Metals and Alloys from Oxides in Fluoride Melts

The success of the Hall Heroult process for the production of aluminum metal from aluminum oxide in a fluoride bath led to attempts by several investigators to obtain rare earth metals and alloys from oxides in halide melts (16). Due to the high melting temperatures of rare earth metals like yttrium, gadolinium and dysprosium, it was extremely difficult to prepare these metals with high purity by fused salt electrolysis. The high working temperatures (1573K) of the cell created numerous problems like higher reactivity of the metal with electrolyte, carbon contamination and higher volatility of electrolyte (16). In the case of samarium metal, although the melting point was low (1300K),direct deposition of metal was less successful, due to the formation of a stable samarium salt (17).

Table 1. SOLUBILITY OF OXIDES IN FLUORIDE MELTS

OXIDE	ELECTROLYTE COMPOSITION	TEMP (K)	OXIDE SOLUBILITY (Wt. %)	X_{MxOy}	$\ln X_{MxOy}$	REFERENCE
Nd_2O_3	90NdF_3-10LiF	1373	2.0	.0071	-4.947	16
	80NdF_3-20LiF (wt. ratio)	1373	2.0	.0051	-5.277	16
UO_2	40UF_4-57BaF_2-3LiF	1523	4.0	.026	-3.647	
	40UF_4-45BaF_2-15CaF_2	1523	3.8	.0238	-3.737	18
CeO_2	63CeF_3-16BaF_2-21LiF	1123	2.0	.00945	-4.662	18
	- do -	1073	1.7	.00803	-4.824	18
La_2O_3	70LaF_3-10$BaF_2$20LiF	1223	2.3	0.00518	-5.264	18
	84LaF_3-16LiF	1223	2.6	.00761	-4.88	18
Y_2O_3	3LiF. YF_3	1013-1318	$\ln X_{Y_2O_3} =$	- 2.878 -	$\frac{3396.9}{T}$	19
	LiF. YF_3	1173-1318	$\ln X_{Y_2O_3} =$	- 1.266 -	$\frac{4143.1}{T}$	19

Several investigators have reported the successful deposition of metals by forming low melting alloys. Generally three methods have been used for the production of rare earth alloys by electrolysis:

a) Electrodepositing the rare earth metal into a liquid cathode pool by alloying with a lower melting metal such as cadmium, zinc, magnesium and aluminum.

b) Electrodepositing rare earth metal on a solid metal cathode to form a liquid alloy.

c) Codepositing metals from mixtures of respective oxides.

Bratland and Grojtheim(19) measured the current density of Y-Mg and Y-Al cathodes as a function of electrolyte composition. An optimum current density of 0.5 A/cm^2 for Y-Mg alloys in equilibrium with the electrolyte composition of 3 $LiF.YF_3$ at 1033K was obtained. The rate at which yttrium metal formed was found to be higher than the rate of transport of yttrium into the bulk cathode. Production of alloys with composition of 49 to 51% Y in Y-Mg and 28 to 72% Y in Y-Al alloy containing $LiF.YF_3$ electrolyte in the temperature range of 998 to 1373K were reported. Boe (20) reported the maximum yield of 27.93% Y in Y-Al at 1273K with 3 $LiF.YF_3$ electrolyte. The rate determining step was the transport of YAl_2 from the cathode surface into the bulk of the cathode alloy. The current efficiency of the cell was increased by increasing the specific density of the electrolyte, decreasing cathode current density and stirring the cathode pool.

Several reports (16, 17, 20, 21) were published on production of rare earth metals Dy, Gd, La, Ce, Nd, Sm, Pr, Y or mischmetal using consumable cathode metals Fe, W, Ni, Mn and Cr with ReF_3.LiF electrolyte mixture containing the oxide feed. Current efficiencies in the range of 27 to 78% were achieved. They concluded that the lower efficiencies are due to 1) the higher reactivity of metal with the electrolyte and 2) the higher stability of the divalent salt (17). Codeposition of Y-Al alloy from a mixture of Y_2O_3 and Al_2O_3 feed in $LiF.YF_3$ melt was reported (20).

Aamland et al. (22) developed a floating magnesium cathode cell for preparing Y-Mg alloy using Y_2O_3 inside feed in a mixture of $3LiF.YF_3$ electrolyte. Alloys with yttrium content as high as 55.6% were prepared. The current efficiency varied from 25.8 to 60.3%. The maximum current efficiency was obtained in the temperature range of 1073 to 1173K at a cathode current density less than 2 A/cm^2. Butorov and Novikov (23) prepared yttrium-zinc alloys with 1.2 to 3.9% Y using a mixed chloride-fluoride melt. A current efficiency of 90% was reported in the current density range of 0.07 to 0.17 A/cm^2.

3.0 SOLUBILITY OF LITHIUM OXIDE IN LiF-CaF_2 MELTS

3.1 Preliminary Analysis

The phase diagram of the Al-Li system (24-26) contains an eutectic occurring at 9.9 wt. % (30 mole %) Li with a melting point of 873K. Liquid compositions exist between pure aluminum and alloy (86 wt. % Al - 14 wt. % Li) at a temperature of 933K. The phase diagram of the LiF-CaF_2 system (25,27) has a single eutectic at 55.6 wt. % LiF (79 mole %) and 44.4 wt. % (21 mole %) CaF_2 with a melting point of 1033K.

3.2 Experimental

The solubility of lithium oxide (Li_2O) was investigated as a function of temperature in the range of 1058 to 1133K in 4LiF.CaF_2 electrolyte. The liquidus freezing temperature of ternary Li_2O-LiF-CaF_2 melt was measured. The experimental methods used and the results obtained are discussed in the following sections.

3.2.1 Materials

Calcium Fluoride (99.9%) pure was obtained from Fisher Scientific Co., Lithium Fluoride (99.9%) pure was obtained from Foote Mineral Co., PA and Lithium Oxide (99.8%) pure and < 0.6 cm size was obtained from Cerac Inc., Milwaukee, WI.

3.2.2 Procedure

The apparatus used for the solubility studies consisted of a 11.5 cm diameter stainless steel chamber with ports for evacuation,

argon gas outlet and for oxide additions. The chamber was heated by a 10cm diameter Kanthal wire-wound cylindrical resistance furnace. A sectional view of the set up used for solubility studies is given in Figure 1.

Calcium fluoride and lithium fluoride were weighed and mixed in stoichiometric proportions of 4:1 to form 75 grams of CaF_2-LiF mixture. The mixture was dried in dynamic vacuum at 423K for 6 hours and then melted at 1073K under a dry argon atmosphere for one hour in a graphite crucible. As shown in fig. 2, commercial argon gas is passed through a train of concentrated sulfuric acid and anhydrous calcium chloride and then through two heated alumina tubes containing copper and titanium chips respectively to maintain a dry argon atmosphere in the chamber.The liquid electrolyte mixture did not wet the graphite crucible and lost in the form of vapors only 0.2 to 0.3% of its original weight after melting. The solidified mixture was crushed and remelted under dry argon atmosphere at the required temperature till a homogenous melt was obtained.

The temperature of the melt was measured by immersing a Pt-Pt/Rh 10% thermocouple connected to a digital thermometer with a resolution of 0.1K and all experiments were done by placing the crucible in the constant temperature zone of the furnace. A sample of the melt was withdrawn through a graphite tube. Lithium oxide, 20% by weight of electrolyte mixture (15 g) was added to the melt. The molybdenum tube containing purified argon gas was passed at a rate of 60 to 80 cm^3/min

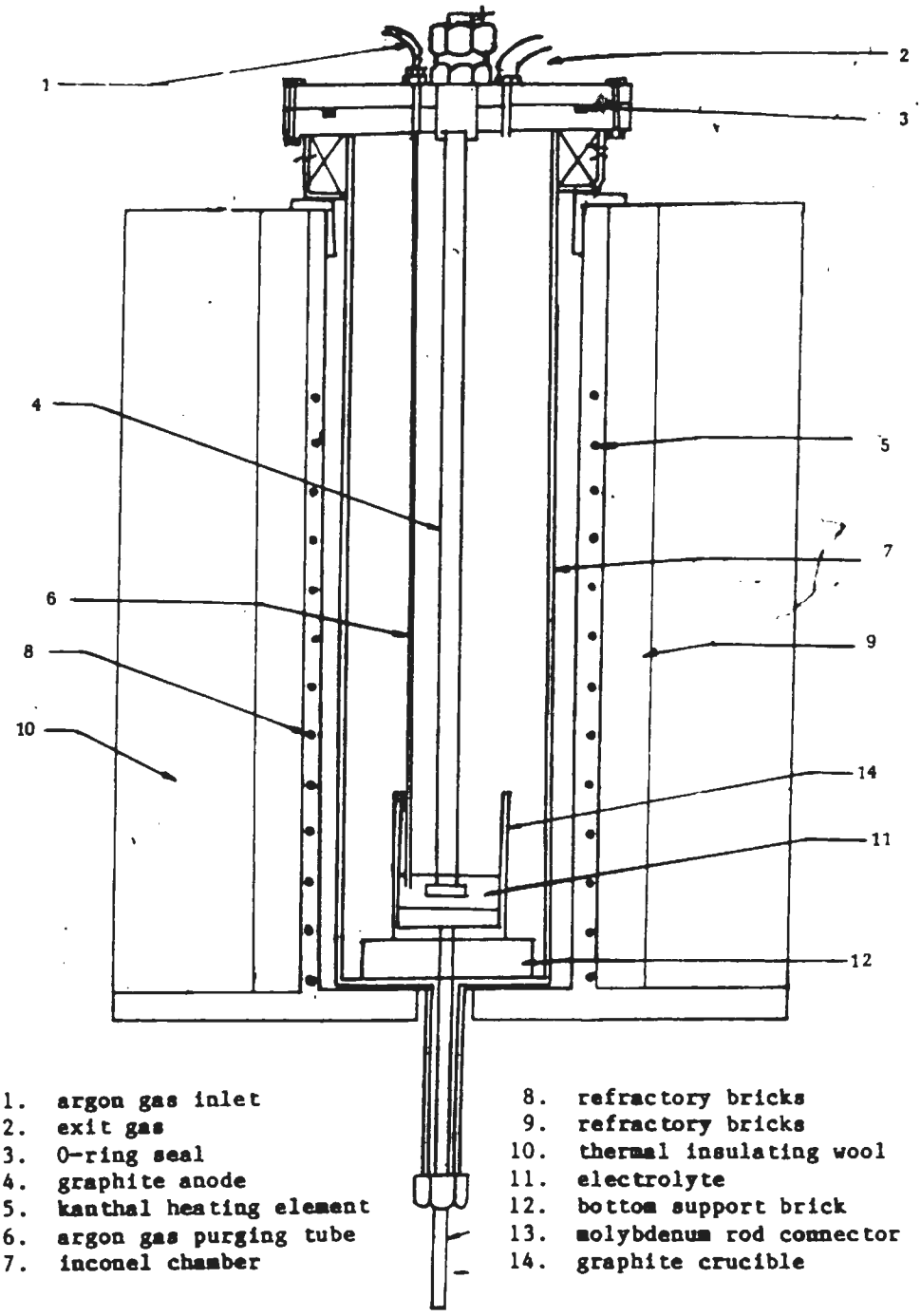

1. argon gas inlet
2. exit gas
3. O-ring seal
4. graphite anode
5. kanthal heating element
6. argon gas purging tube
7. inconel chamber
8. refractory bricks
9. refractory bricks
10. thermal insulating wool
11. electrolyte
12. bottom support brick
13. molybdenum rod connector
14. graphite crucible

FIG. 1 SECTIONAL VIEW OF SETUP FOR ELECTROLYSIS EXPERIMENTS

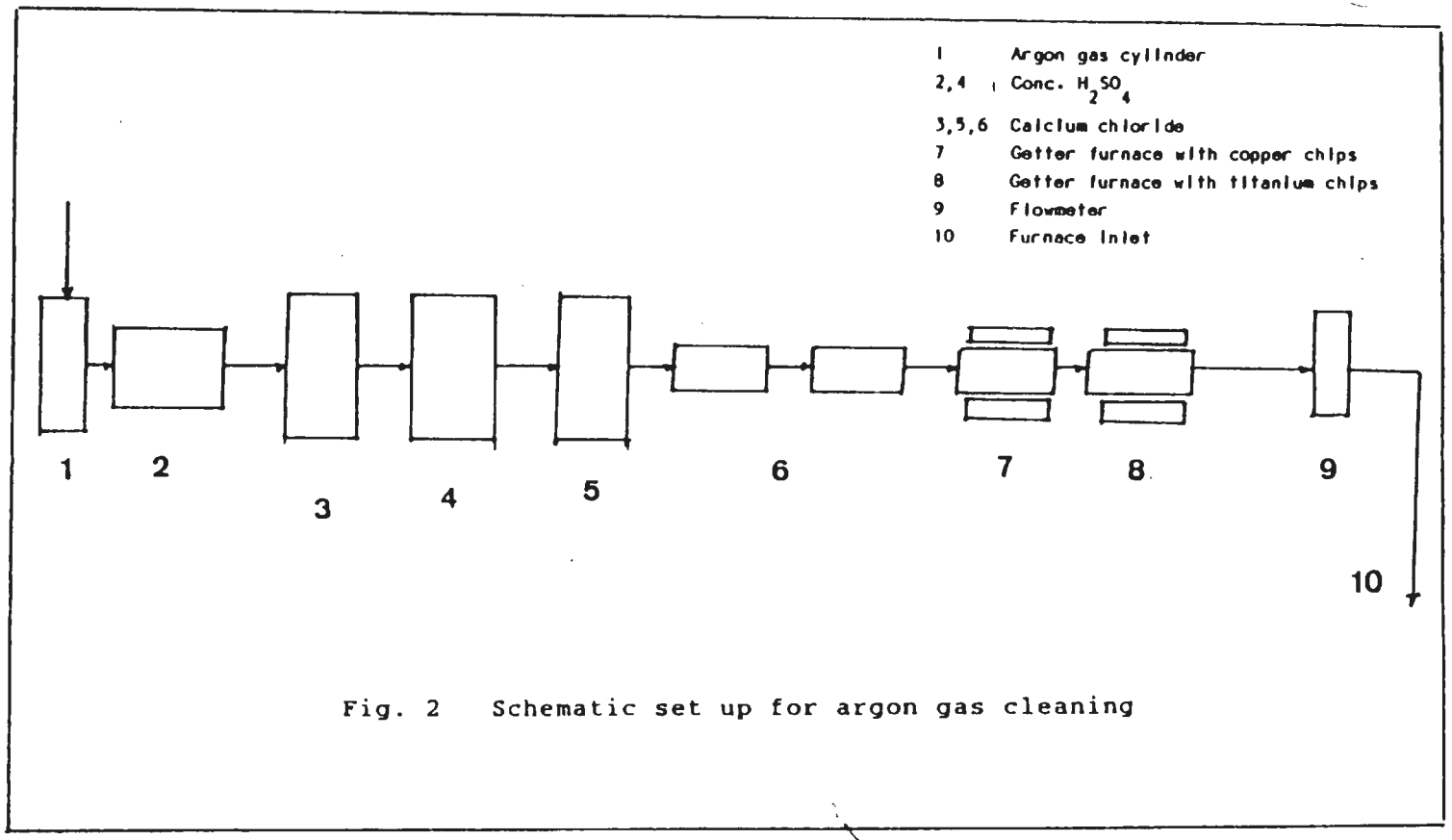

Fig. 2 Schematic set up for argon gas cleaning

by immersing into the melt to provide a stirring effect. Samples were withdrawn through a graphite tube at selected time intervals after the addition of oxide. At least 10 minutes prior to each sampling, the Molybdenum tube was lifted above the melt to allow the undissolved oxide particles to settle. The solidified samples were ground to less than 100 mesh size in an alundum vial, to obtain a homogenized mixture and the powder was analysed for the constituent elements, i.e. Ca, Li, F, and O.

3.2.3 Chemical Analysis

Chemical analysis of the individual elements formed a critical part of the investigations. An inert gas fusion technique was used for the determination of Oxygen. A LECO oxygen analyser was used. The method (18) consisted of reacting the sample with a graphite crucible at about 2273K. The CO gas evolved was passed through a series of traps to absorb the volatalized fluorides. The oxygen level in the sample was determined by comparing with a purified helium gas stream by thermal conductivity methods. Three determinations were made for each sample and the average values were reported. An error of $\pm$0.5% in the measurement of oxygen values were reported. Samples withdrawn prior to the addition of Li_2O had a blank of 0.12 to 0.16 wt. % oxygen. All samples were dried in dynamic vacuum at 423K for 6 hours prior to analysis. Calcium and Li were analysed by atomic absorption spectrophotometry by dissolving the samples in $AlCl_3$-HCl solution (28). Interferences from Al were reduced by additions of 1% potassium as KCl. A nitrous oxide-acetylene flame was used for the determination of Ca.

Fluorine was determined by selective ion electrode method using a Corning Fluoride electrode (28).

X-ray diffraction studies were performed on the solidified electrolyte samples. A copper Kα radiation (λ = 1.5405 A°) was used. X-ray diffraction patterns of the samples were compared with reagent grade (99.9% purity) LiF, CaF_2, Li_2O and synthetic $4LiF.CaF_2$ mixture. All samples showed no evidence of undissolved Li_2O or any other Li compounds, indicating oxygen in the melts were totally in the dissolved form.

3.2.4 Liquidus Temperature of 4LiF CaF_2 +Li_2O (sat.)

In order to determine the optimum temperature for electrolysis of Li_2O in 4LiF CaF_2 melts, the liquidus temperature of 4LiF CaF_2 + Li_2O (sat) melt was determined. The same set up as given in Figure 1 was used. Temperature was measured by a 0.04 mm diameter Pt-Pt/13%Rh thermocouple enclosed and grounded by a thin inconel sheath. The melt was held at 1093K for 6 hours to make sure the complete solution is formed after the addition of excess Li_2O. The melt was cooled at the rate of 0.5 degree K/minute by adjusting the temperature controller setting. The melt was kept stirred by bubbling purified argon gas through a molybdenum tube throughout the experiment at the rate of 100 cm^3/min. Three sets of heating and cooling cycles were performed. A liquidus temperature of 1004.5 $\pm$ 2.5 was obtained with a thermal arrest time of 3.5 to 4.6 minutes as shown in Table 2. The cooling curve for the sample showing a thermal arrest temperature of 1006K and a thermal

TABLE 2. LIQUIDUS TEMPERATURE OF $4LiF.CaF_2 + Li_2O$ (sat.) MELT

Melt Composition	Liquidus Temp (K)	Thermal Arrest Time (min)
$4LiF.CaF_2 + Li_2O$(sat)	1005 ± 1	3.5
"	1006 ± 1	4.6
"	1003 ± 1	3.8

arrest time of 4.6 minutes is shown in figure 3.

3.3 Results and Discussion

The solubility of Li_2O was measured as a function of temperature in the range of 1058 to 1133K and the reaction time of up to 6 hours was found for the eutectic composition of $4LiF.CaF_2$ liquid electrolyte melt. The results showed that about four hours were required to reach the equilibrium saturation of Li_2O with the melt. The experimental data and thermodynamic data of Li_2O in the melt as a function of temperature are presented in Table 3. As seen from the table, the solubility of Li_2O increases with increase in temperature of the melt. For example, the solubility of Li_2O increased from 10.63 wt. % at 1058K to 14.82 wt. % at 1133K. The calculated mole fraction of Li_2O in the melt as a function of temperature is plotted in figure 4. A linear relationship between ln mole fraction of Li_2O and temperature was obtained, and is given by:

$$\ln X_{Li_2O} = 2.411 - \frac{4567.8}{T} \qquad (1)$$

with a correlation coefficient of 0.98.

A comparison of collected values for the solubility of different oxides in fluoride melts is shown in Figure 5. Higher solubility of Li_2O in fluoride melt compared to the other oxides is observed. Because of different molar ratios of oxide to fluoride in the electrolyte, a strict comparison cannot be made among these systems.

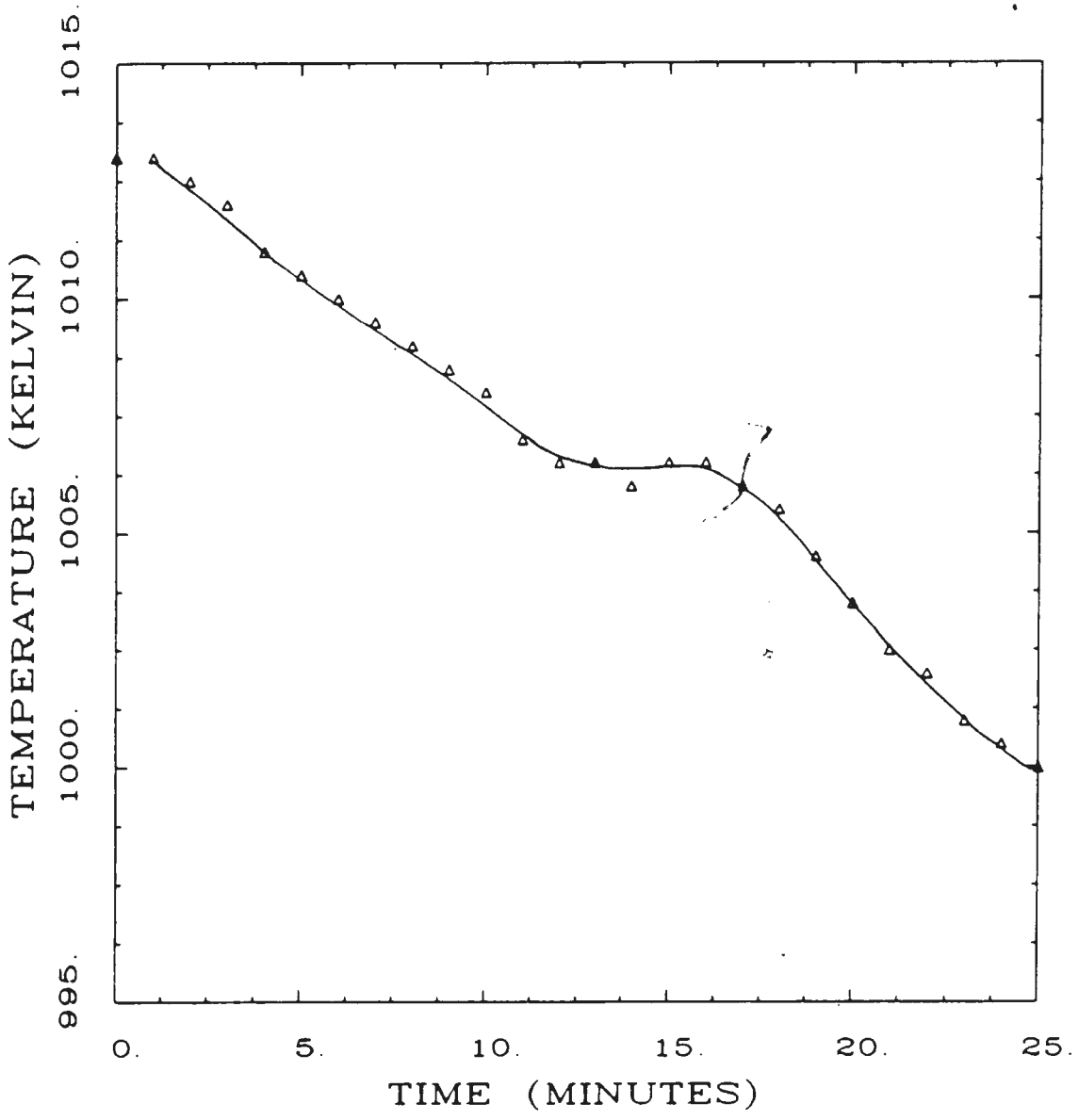

Fig. 3 Cooling curve for $4LiF.CaF_2+Li_2O$(sat.) melt showing thermal arrest at 1006K

TABLE 3. SOLUBILITY, ACTIVITY AND ACTIVITY COEFFICIENT OF Li_2O IN 4LIF.CaF_2 MELTS FOR SEVERAL TEMPERATURES.

Temp (K)	$\frac{1}{T} \times 10^4$ (K^{-1})	Li_2O wt.%	X_{Li_2O}	$\ln X_{Li_2O}$	a_{Li_2O}	γ_{Li_2O}
1058	9.450	10.63	0.147	-1.917	0.080	0.543
1078	9.276	11.66	0.159	-1.839	0.090	0.566
1093	9.149	13.20	0.176	-1.737	0.099	0.563
1113	8.985	14.22	0.187	-1.676	0.111	0.594
1133	8.826	14.82	0.193	-1.645	0.124	0.643

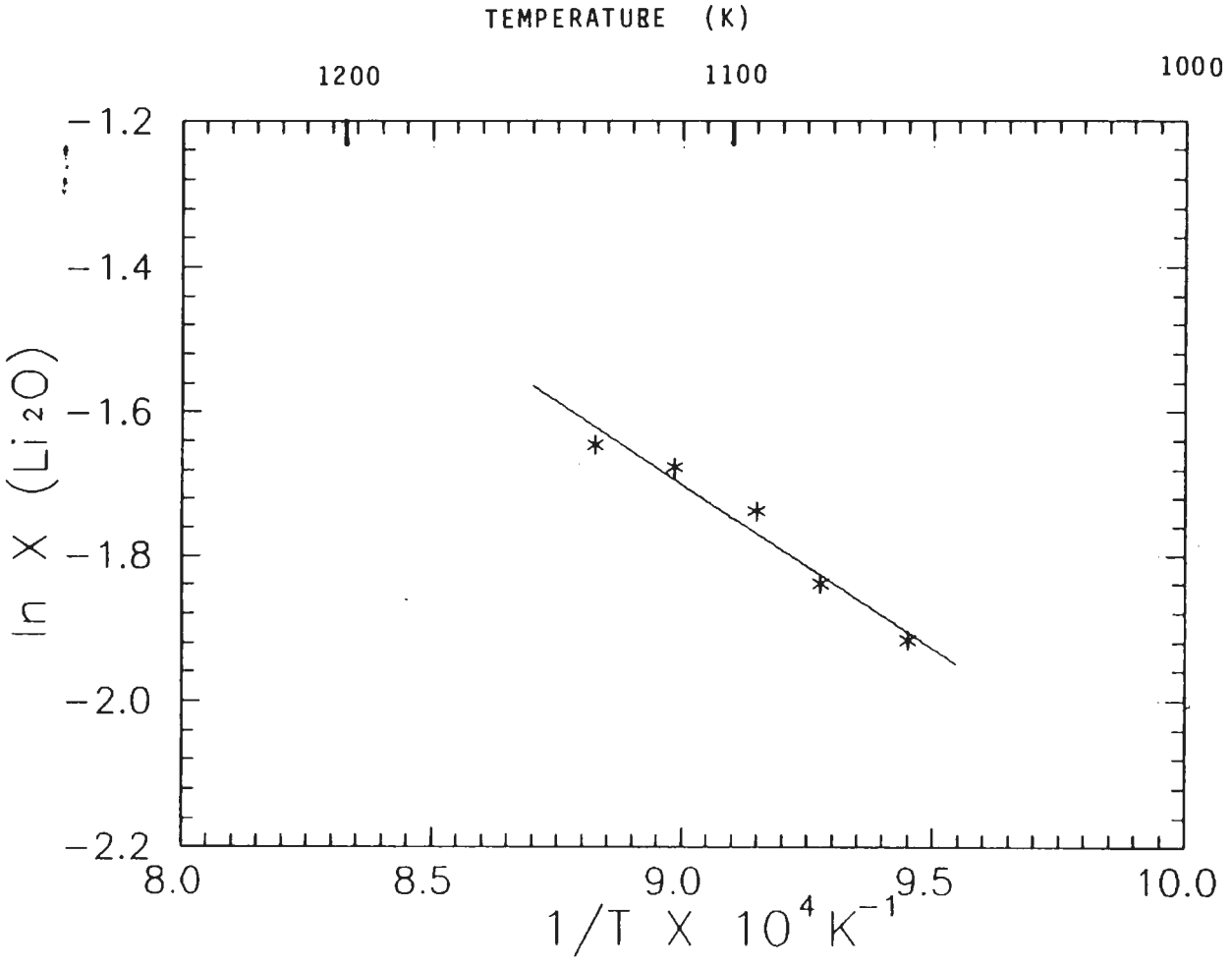

Fig 4. Variation of ln mole fraction of Li_2O in $4LiF.CaF_2$ melt with temperature

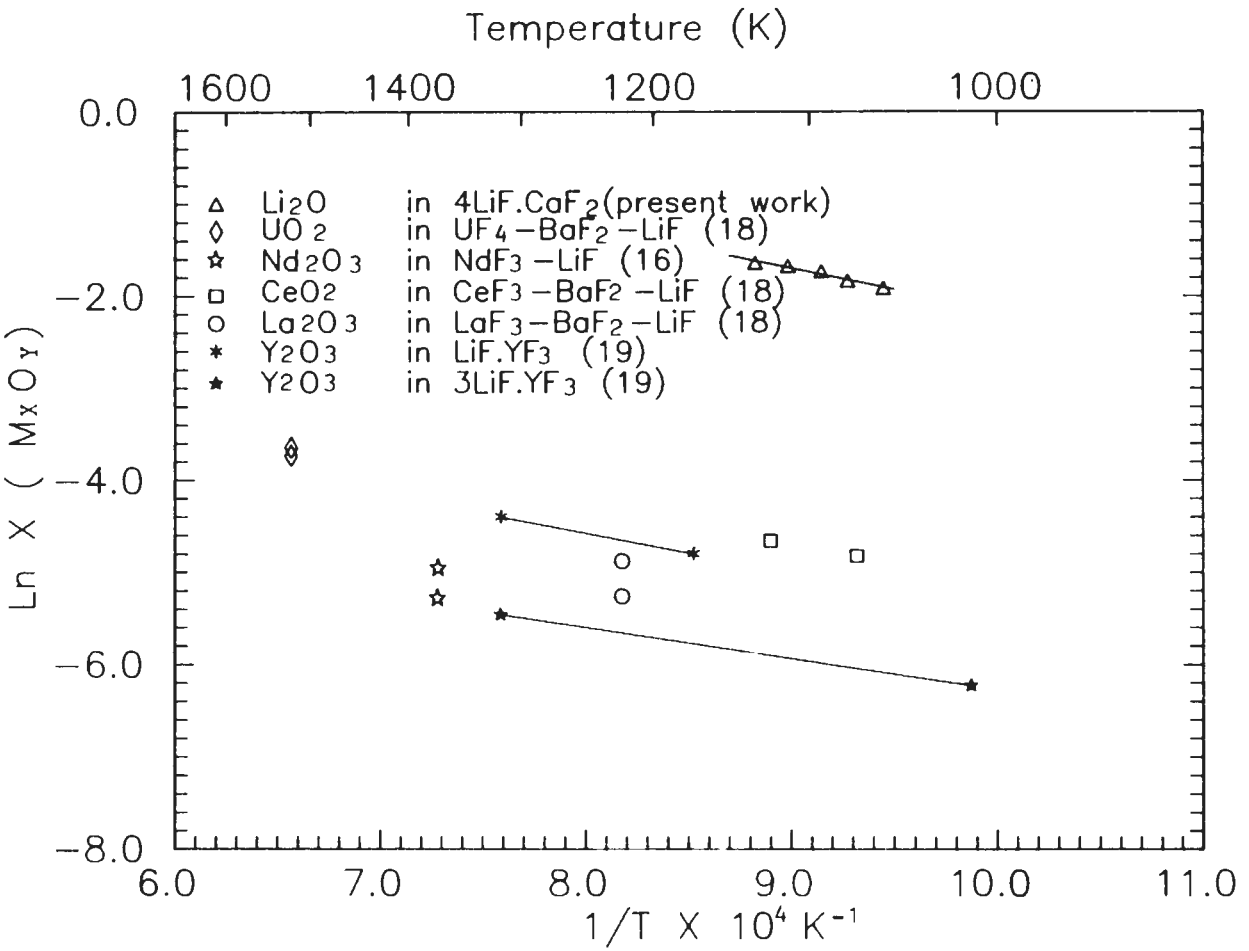

Fig 5. Solubility of metal oxides in fluoride melts as a function of temperature

In general, it can be concluded that at 1100K, the solubility of Y_2O_3 in $LiF.YF_3$ is $0.082X_{Y2O3}$, which is about a factor of two less than the Li_2O ($0.175XLi_2O$) in $4LiF.CaF_2$ melts (21).

3.3.1 Activity of Coefficient of Li_2O:

The melting points of Li_2O and $4LiF.CaF_2$ are 1705 ± 6K (29) and 1042K (27) respectively. The liquidus freezing temperature as reported in the previous section for $4LiF.CaF_2$-Li_2O (saturated) melt is 1004.5 ± 2.5K at 11.77 mole% Li_2O. At any temperature above 1004K, for $4LiF.CaF_2$+Li_2O(sat.) melt, solid Li_2O is in equilibrium with the liquid electrolyte. In other words,

$$Li_2O \text{ (liquid, electrolyte)} \rightleftharpoons Li_2O \text{ (solid)} \qquad (2)$$

The partial molar free energy of Li_2O in the liquid electrolyte $\Delta\bar{G}_{Li_2O(l)}$ should be equal to the molar free energy of the pure solid , $\Delta G^{\circ}_{Li_2O(s)}$ Hence

$$\Delta G_{Li_2O} = \Delta G^{\circ}_{Li_2O(l)} + RT\ln a_{Li_2O(l)} = \Delta G^{\circ}_{Li_2O(s)} \qquad (3)$$

or

$$RT\ln a_{Li_2O(l)} = -\Delta G^{\circ}_{Li_2O(l)} + \Delta G^{\circ}_{Li_2O(s)}$$

$$= -\Delta G^{\circ}_{m,\ Li_2O} \qquad (4)$$

where ΔG°_m is the free energy of fusion of Li_2O at a temperature T. $\Delta G^{\circ}_{m,Li_2O}$ was deduced from the suggested value of heat of fusion $\Delta H_{m,\ Li_2O}$ = 58576 J/mole (30) and melting point of Li_2O. The

following expression was obtained.

$$\Delta G^{\circ}_{m,Li_2O} = 58576 - 34.35\ T\ J/mole \qquad (5)$$

Combining equations 4 and 5, the activity of Li_2O at several temperatures was calculated. From known value of activity, activity coefficient of Li_2O ($\gamma Li_2O = aLi_2O/XLi_2O$) was calculated and are tabulated in Table 3. As seen from the table, dissolution of Li_2O in $4LiF.CaF_2$ electrolyte melt exhibits a non-ideal behavior and follows a negative deviation ($\gamma Li_2O < 1$) from the Raoult's law.

4. ANODIC OVERVOLTAGE ON GRAPHITE DURING ELECTROLYSIS OF Li_2O in $4LiF.CaF_2$ MELT

The anodic overvoltage measurements were made with the standard steady state current voltage method. From the experimental data, Tafel constants, and a possible reaction mechanism via oxyfluoride complexes in the melt were derived. These are discussed in the following sections.

4.1 Experimental

The anodic overvoltage on graphite anode during the electrolysis of Li_2O in $4LiF.CaF_2$ melts was studied. A schematic set up of the furnace and the electrolytic cell is shown in Figure 6. The circuit for the electrolytic cell is shown in Figure 7. The preparation of the chemicals was done as similar to one described in the solubility experiments in section 3.2. The inert gas chamber and the argon gas purification apparatus used was described previously. A graphite anode and a graphite reference electrode (6 mm dia.) was used for the overvoltage measurements. The temperature of the electrolyte was measured by a chromel-alumel thermocouple. The voltage between the graphite anode and the graphite reference electrode was measured by a Hewlett Packard multimeter with an internal resistance of 100 Mohm and the current was measured by the potential drop across a standard resistance with a multimeter. The anodic polarization curve was obtained by increasing the applied current in small steps and holding the current at each step to obtain a steady potential. The current was found to be steady with a scatter of 0.01 ampere.

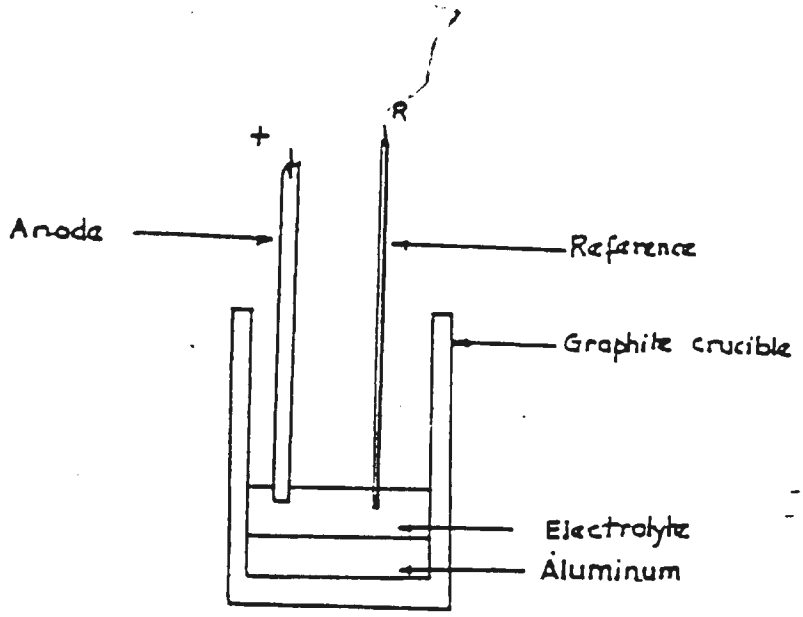

Fig. 6. Schematic cell setup for anodic overvoltage measurements

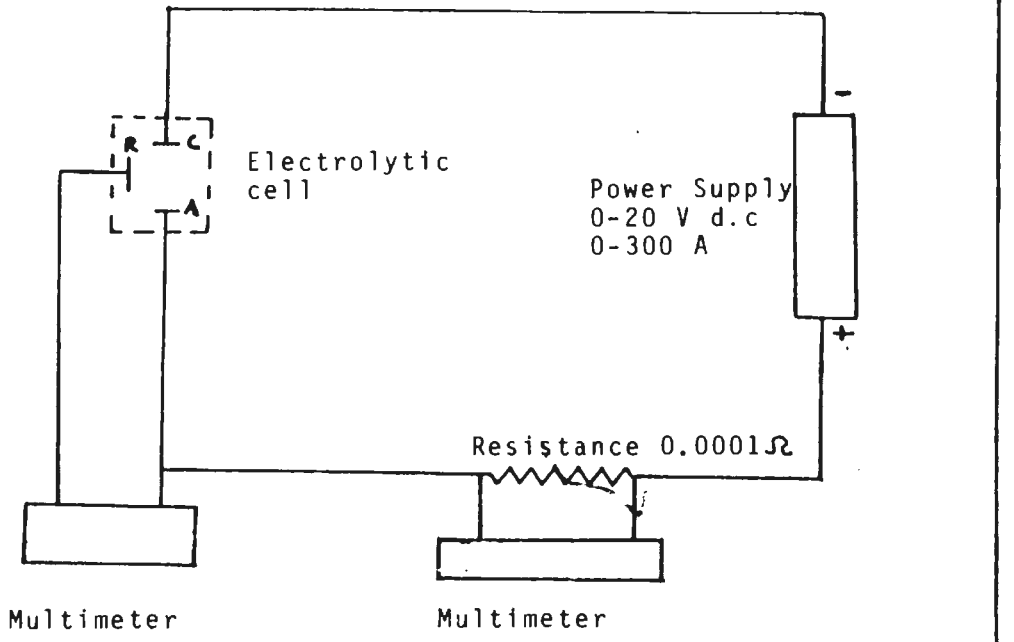

Fig. 7 Electric circuit for electrolytic cell

4.2 Results and Discussion:

The anodic overvoltage on graphite was measured as a function of log current density. The experiments were done in $4LiF.CaF_2$ electro -lyte saturated with Li_2O. Further investigation is needed to study the effect of Li_2O concentration on overpotential. At all temperatures studied, the plot of overvoltage η vs log current density i showed a Tafel relationship (linear dependance of overvoltage on log current density). Such a plot generated from the experimental data (presented in Table 4) at 1103K is shown in Figure 8. A linear dependance of η vs log i was observed up to 0.25 A/cm^2 and a limiting current phenomenon was observed between 0.25 A/cm^2 and 0.40 A/cm^2 where the curve deviated from the straight line. On further increasing the current density, abrupt changes were observed with a sharp change in with a small change in current density. However above 8.0 A/cm^2 the overvoltage increased above 20 volts and sparking could be seen around the anode. This was due to anode effect (20) and the current returned back to very low values. From the straight line region of the curve for η vs log i at 1103K as shown in Figure 8, i.e. Tafel region, the following regression equation was obtained.

$$\eta = 1.01 + 0.30 \log i \qquad (6)$$

Above the limiting current density range (>0.4 A/cm^2), the following regression equation was obtained.

TABLE 4. RESULTS OF ANODIC OVERVOLTAGE MEASUREMENTS AT 1103 K

Potential (volts)	Current (Amperes)	Current Density(i) ($Amp./cm^2$)	log i
0.040	0.002	3.80×10^{-3}	-3.420
0.186	0.027	5.13×10^{-3}	-2.900
0.252	0.034	6.46×10^{-3}	-2.189
0.315	0.051	9.51×10^{-3}	-2.022
0.393	0.067	0.013	-1.886
0.485	0.102	0.019	-1.721
0.520	0.132	0.025	-1.600
0.558	0.165	0.031	-1.503
0.580	0.211	0.040	-1.397
0.616	0.253	0.048	-1.318
0.639	0.280	0.053	-1.272
0.663	0.386	0.074	-1.134
0.704	0.478	0.091	-1.042
0.727	0.609	0.115	-0.940
0.745	0.903	0.172	-0.765
0.840	1.165	0.222	-0.655
0.912	1.362	0.259	-0.587
0.946	1.802	0.343	-0.465
0.967	2.150	0.409	-0.389
1.040	2.550	0.484	-0.315
1.130	2.940	0.559	-0.253
1.240	3.010	0.572	-0.242

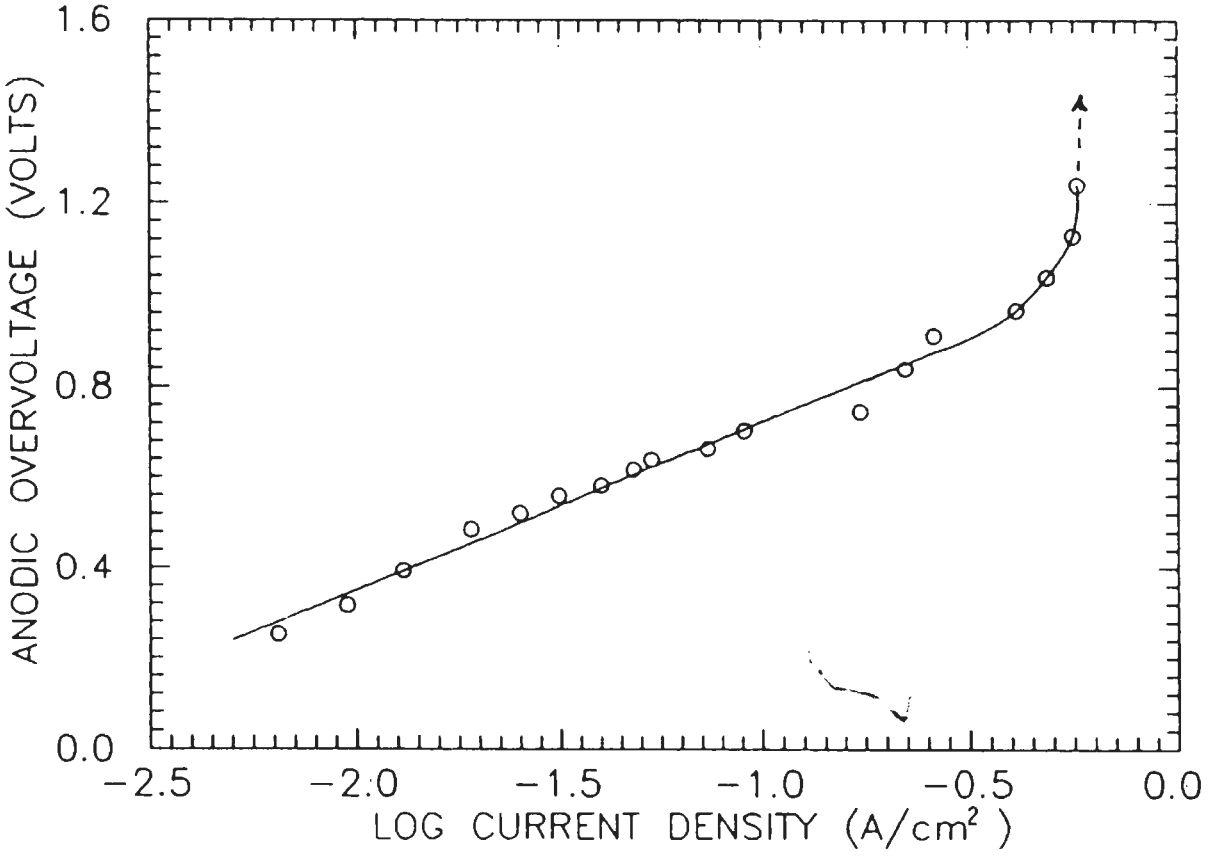

Fig 8. Log current density as a function of overvoltage on graphite during electrolysis of $4LiF.CaF_2 + Li_2O$ (sat.) melt at 1103K

$$\eta = 1.58 + 1.62 \log i \qquad (7)$$

Experimental data was analysed by considering an anode reaction mechanism consisting of the following two steps (20):

I. Reaction between oxygen-carrying complex and anode, with the transfer of two electrons:

$$LiO_xF^{-2} + C(gr) = LiF + CO_x\ (g) + 2\bar{e} \qquad (8)$$

where x=1 for CO(g) and x=2 for CO_2(g).

II. Desorption of adsorbed CO_x:

$$CO_x(ad) = CO_x(g,\ 1\ atm) \qquad (9)$$

The equation relating current density and anode potential for step I (31) can be written as:

$$i = K^+C^2\ (1-\theta)\ \exp\left(\frac{2\alpha FE}{RT}\right) - K^-\ \theta\ \exp\left(\frac{-2(1-\alpha)FE}{RT}\right) \qquad (10)$$

where, C is the concentration of the oxygen-carrying complex LiO_xF^{-2}, K^+ and K^- are the rate constants for the anodic and cathodic reactions, θ is the surface coverage of CO_x(ad), E the anode potential, α the transfer coefficient, R the gas constant, T the absolute temperature and F Faradays constant. By introducing the exchange

current density i_o and rearranging equation 10, we obtain equations 11 and 12.

$$i_o = K^+ C^2(1-\theta_o) \exp\left(\frac{2\alpha F E^\circ}{RT}\right) \quad (11)$$

$$i_o = K^- \theta_o \exp\left(\frac{-2(1-\alpha)F E^\circ}{RT}\right) \quad (12)$$

and the overvoltage

$$\eta = E - E^\circ \quad (13)$$

Equation 10 transforms to:

$$i = i_o\left[\left(\frac{1-\theta}{1-\theta_o}\right) \exp\left(\frac{2\alpha F\eta}{RT}\right) - \frac{\theta}{\theta_o} \exp\left(\frac{-2(1-\alpha)F\eta}{RT}\right)\right] \quad (14)$$

Assuming a surface coverage $\theta=\theta_o$ (i.e., no accumulation of produced CO_x) equation 14 reduces to equation 15:

$$i = i_o\left[\exp\left(\frac{2\alpha F\eta}{RT}\right) - \exp\left(\frac{-2(1-\alpha)F\eta}{RT}\right)\right] \quad (15)$$

For high anodic current densities equation 15 can be written as:

$$\eta = -\frac{2.303RT}{2\alpha F} \log i_o + \frac{2.303RT}{2\alpha F} \log i \quad (16)$$

$$\text{or} \quad \eta = a + b \log i \quad (17)$$

Equation 16 is the usual Tafel equation for a charge-transfer controlled two electron reaction. Slope of the plot of η vs log i for the experimental data gives the value of Tafel constant, $\left(b = \frac{2.303RT}{2\alpha F}\right)$ and intercept gives constant $a\left(= -2.303 \frac{RT}{2\alpha F} \log i_o\right)$.

From the experimentally derived value of a and b, the exchange current density and charge transfer coefficient was determined.

Comparing equation 17 and 6, the Tafel constants a and b were deduced as 1.01 and 0.30 respectively.

At higher current densities, beyond the Tafel limit, the plot of log current density and overvoltage followed a non-linear relationship. This might be caused by a slow desorption of adsorbed CO_x on the anode, Viz. Step II.

A Langmuir adsorption behavior for CO_x is assumed, and the rate of Step II can be expressed as:

$$i = K_d\,\theta - K_a\,P_{CO_x}\,(1-\theta) \qquad (18)$$

where K_d and K_a are rate constants for desorption and adsorbtion of CO_x, θ the surface coverage of CO_x (ad) and P_{CO_x} the partial pressure of CO_x gas. A limiting current phenomenon will occur when $\theta \to 1$. The value of the "exchange current density" for Step II, at equilibrium, the equation reduces to equations 19 and 20:

$$i_r = K_d\,\theta_o \qquad (19)$$

$$i_r = K_a\,P_{CO_x}\,(1-\theta_o) \qquad (20)$$

Substituting equations 19 and 20 in 18 and rearranging, we obtain equation 21.

$$i = i_r \left[\frac{\theta}{\theta_o} - \frac{(1-\theta)}{(1-\theta_o)}\right] \qquad (21)$$

Solving equation 23 with respect to θ gives:

$$\theta = \frac{i}{i_r}\,\theta_o\,(1-\theta_o) + \theta_o \qquad (22)$$

Under the assumption that α = 1/2, the equation 14 reduces to equation 23.

$$i = i_o \left(\frac{1-\theta}{1-\theta_o}\right) \exp\left(\frac{F\eta}{RT}\right) - \frac{\theta}{\theta_o} \exp\left(\frac{-F\eta}{RT}\right) \qquad (23)$$

Substituting θ value from equation 22 in 23, and omitting the cathodic term in equation 23 gives:

$$\frac{1}{i} = \frac{1}{i_o} \exp\left(-\frac{F\eta}{RT}\right) + \frac{\theta_o}{i_r} \qquad (24)$$

The slope of the plot $\frac{1}{i}$ vs $\exp\left(\frac{-F\eta}{RT}\right)$, the exchange current i_o of Step I was determined. From the intercept with the ordinate in the above plot, the constant term in equation 24 was determined. By substituting the θ_o/i_r value in equation 22, the limiting current i_L was calculated when θ->1 (limiting current phenomenon occurs).

Using the experimental data (linear region of Figure 8), the exponential term on the right side of equation 24 i.e. $\exp\left(-\frac{\eta F}{RT}\right)$ was calculated. These values are presented in Table 5. From the plot of $\frac{1}{i}$ as a function of $\exp\left(-\frac{\eta F}{RT}\right)$, as shown in Figure 9, by linear regression, the following relationship was obtained:

$$\frac{1}{i} = 1.22 \times 10^4 \exp\left(-\frac{\eta F}{RT}\right) + 2.63 \qquad (25)$$

The correlation coefficient is equal to 0.988. Current densities in the range of 0.04 and 0.259 A/cm^2 from Table 4 were used to plot Figure 9. By comparison of equations 24 and 25, θ_o/i_r and i_o values

TABLE 5. SUMMARY OF LIMITING CURRENT DENSITY CALCULATIONS AT 1103K

η (volts)	i (Amperes/cm^2)	$\frac{1}{T}$	$\exp\left(-\frac{F\eta}{RT}\right)$
0.580	0.040	25.00	2.237×10^{-3}
0.616	0.048	20.83	1.532×10^{-3}
0.639	0.053	18.86	1.203×10^{-3}
0.663	0.074	13.51	9.342×10^{-4}
0.704	0.091	10.99	6.068×10^{-4}
0.745	0.174	5.81	3.942×10^{-4}
0.840	0.222	4.50	1.451×10^{-4}
0.912	0.259	3.861	6.800×10^{-5}

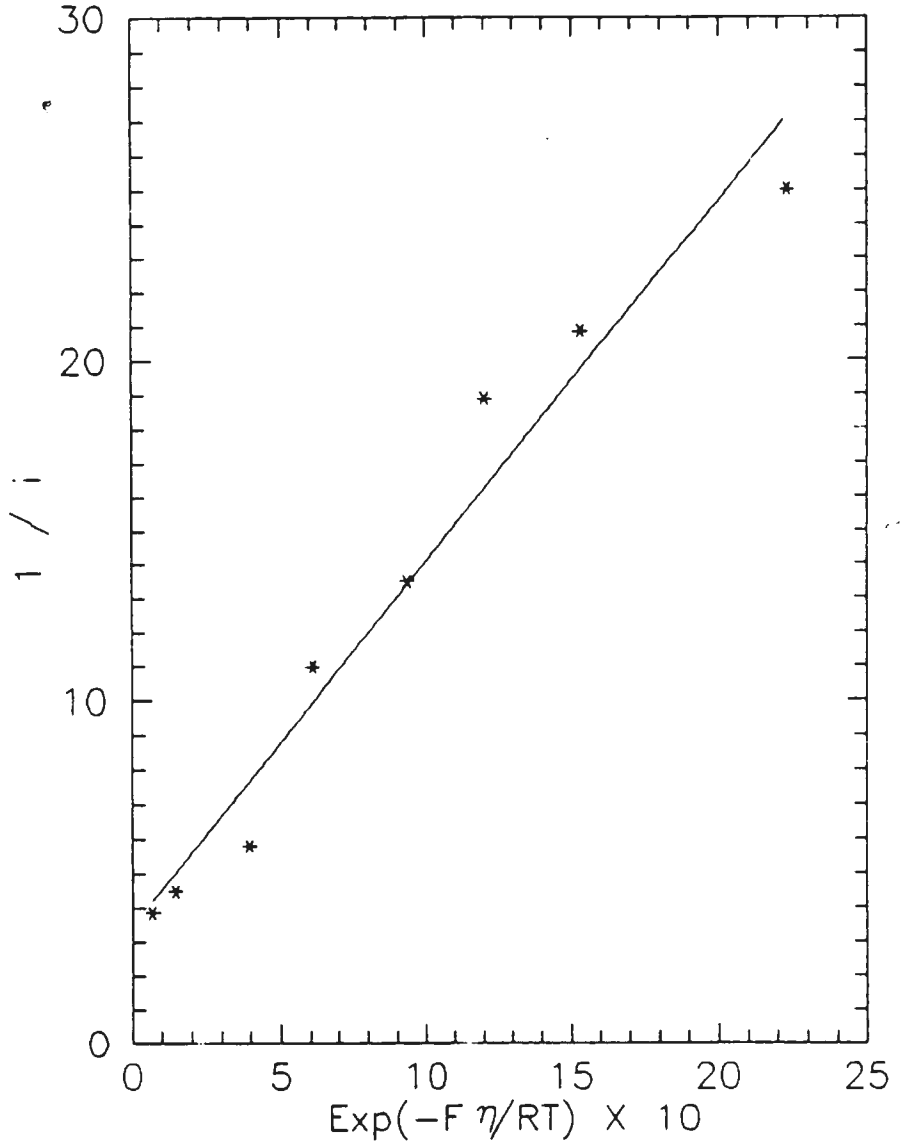

Fig 9. Current density as a function of Exp(−F η/RT) at 1103K

were determined to be 2.63 and 8.21 $x10^{-5}$ respectively. As discussed above, substituting θ_o/i_r value in equation 24 and setting $\theta \to 1$, (i.e. $\theta_o << 1$), it reduces to:

$$2.63\ i_L = 1 \qquad (26)$$

or

$$i_L = 0.38\ A/cm^2$$

This value of limiting current density is within the range of experimentally observed value of 0.25 to 0.4 A/cm^2. The effect of stirring rate on the anodic overpotential curve was studied qualitatively and it was found that the overpotentials and the limiting current density was independant of the stirring rate.Further there were no fluctuations in the current in the limiting current density region. If the rate limiting step was due to mass transfer of electrolyte through a diffusion boundary layer, the limiting current density would have increased with increased stirring rate and fluctuations in the current in the limiting current density region due to changes in the diffusion boundary layer thickness would have been observed. Hence it can be inferred that diffusion through the electroyte is not rate controlling and the limiting current phenomenon is predominantly due to a blockage effect caused by adsorption of CO on the anode surface.

4.2.1 Determination of Oxyfluoride Complex, ($LiOxF^{2-}$):

The gases formed at the graphite electrode with the addition of Li_2O to the electrolyte are CO and or CO_2. At the reaction temperature of 1103K, the composition of the gaseous mixture can be calculated as follows:

Consider the reaction at the graphite electrode

$$C(gr) + CO_2(g) = 2CO(g) \qquad (27)$$

ΔG° (at 1103K) = -22033.5 J/mole (30)

Equilibrium constant K is written as

$$K = \frac{P_{CO}^2}{P_{CO_2} a_C} = \frac{P_{CO}^2}{P_{CO_2}} \qquad (28)$$

where a_C=1 for graphite electrode.

For a total pressure of 1 atm

$$P_{CO} + P_{CO_2} = P_T = 1 \text{ atm} \qquad (29)$$

Combining equations 28 and 29 and expressing in terms of CO, the following equation 30 can be obtained:

$$P_{CO}^2 + 11.0535\, P_{CO} - 11.0535 = 0 \qquad (30)$$

solving the equation 30 by quadratic method, P_{CO} = 0.923 atm and P_{CO_2} = 0.077 atm are deduced. Above calculations indicate both CO and small amount of CO_2 gases are generated during the reaction in the melt. The reaction 8 in Step I then can be written for CO and CO_2 gases as

$$LiOF^{2-} + C(gr) = LiF + CO(g) + 2e^- \quad (31)$$

and

$$LiO_2F^{2-} + C(gr) = LiF + CO_2(g) + 2e^- \quad (32)$$

A theoretical estimation of Tafel constant b, given by equation 16 can be made. Considering transfer coefficients α_c (cathode) = α_a ($=1-\alpha_c$) (anode) = 1/2, and from the above equations number of electrons in the reaction is equal to 2, gas constant R = 8.314 J/mole K, Faraday constant, F = 96486.8 J/volt. g equivalent and at temperature of the melt, T = 1103 K, the value of b = 0.22 was calculated. Since the gas mixture contains both CO and CO_2 at different ratios, the contribution of CO to b is (0.218x0.923) 0.20 and CO_2 is (0.218x0.077) 0.02.

The Tafel constant b derived from the experimental data (b = 0.30) is higher than the theoretically estimated value (0.22). But it is in good agreement with the Tafel constant b = 0.22 to 0.28 V derived from the studies on graphite in cryolite melts (32). Using α = 1/2 and two electrons, the exchange current density i_o was calculated from Tafel constant a in equation 6 is $i_o = 4.68 \times 10^{-4}$ A/cm^2. This is an order of

magnitude higher than the i_o value calculated by equation 25, 8.21×10^{-5} A/cm^2. From the above analysis it can be predicted that the melt is composed of LiO_xF^{2-} oxyfluoride complex. Namely, 92.3 % of $LiOF^{2-}$ and 7.7 % of LiO_2F^{2-} complexes at 1103K in $4LiF.CaF_2$ - Li_2O melts.

5.0 ELECTROLYSIS OF Li_2O IN $LiF-CaF_2$ MELTS TO ALUMINUM LITHIUM ALLOYS

Efficiency of the Electrolytic Process:

The efficiency of electrolysis as a function of temperature and composition of the electrolyte was determined.

The efficiency of the cell in terms of cathode current efficiency, K_{A-h}, is defined as:

$$K_{A-h} = \frac{\text{Theoretical ampere-hour required}}{\text{Actual ampere-hour required}} \quad (33)$$

for the same quantity of Li deposited

$$(I\ t)_{ac} = \frac{(I\ t)_{th}}{K_{A-h}} \quad \text{Ampere-hours per ton of Li} \quad (34)$$

Energy consumption of the process:

$$W = V(It)_{ac} \times 10^{-3} \text{ KWH/ton} \quad (35)$$

where I = current, V = cell voltage, t = time required for production of one ton of Li, substituting (I t)ac from equation 36, in 37, we obtain equation 38.

$$W = \frac{V(I\ t)th \times 10^{-3}}{K_{A-h}} \text{ KWH/ton} \quad (37)$$

The solubility of Li_2O in the electrolyte, liquidous freezing point, and anode overvoltage data derived in the previous sections was used in carrying out the efficiency experiments, which are discussed in the following section.

5.1 Experimental

The same furnace and inert atmosphere chamber used for the anodic overvoltage measurements was used for the electrolysis experiments. A schematic diagram of the furnace and the electrolytic cell is shown in Figure 1. The temperature was measured by a Chromel-Alumel thermocouple connected to an OMEGA digital readout temperature indicator which has a resolution of one degree centigrade.

A graphite crucible of 7 cm I.D., 0.6 cm wall thickness and 1.27 cm thick bottom was used for all experiments. The anode consisted of a 3.80 cm dia. and 61 cm long graphite rod, threaded to a graphite disk 2.54 cm in diameter to obtain sufficient current density (1-2 A/cm^2). The dc power source consisted of a silicon controlled rectifier with a maximum dc power output of 20V and 300A. The electrodes were connected to the rectifier by copper connectors and welding quality cables capable of carrying current up to 200A. While a molten pool of aluminum serves as the cathode, connection between the graphite crucible and cable is made through a molybdenum rod 1 cm in diameter. The rectifier can produce a constant voltage of 0-20V$\pm$ 10mV and was read by a digital multimeter. The current was measured by the potential drop across a standard resistance (.001 ohm) connected to a Hewlett Packard digital multimeter which has an internal resistance of 100 M ohm. The multimeter reads currents to an accuracy of $\pm$ .01 ampere.

The electrolyte constituents, CaF_2 and LiF were mixed in the stoichiometric proportions and dried in vacuum overnight at 393 K.

About 180 g of mixture was used for each experiment. About 150 g of granular aluminum (99.9% pure) was used. The depth of liquid aluminum was 1.3 cm and that of molten electrolyte was 1.8 cm. A weighed quantity of lithium oxide was added to the electrolyte to obtain a melt saturated with Li_2O. After about two hours of stirring by argon gas, the graphite anode was slowly lowered into the electrolyte. The graphite disk was completely immersed into the electrolyte and the electrolysis was started by applying a potential of 4-5 volts to enable a current of at least 30 amps (>1 amp/cm^2 current density) to be produced. The applied potential and current was recorded at intervals of one minute till the current fell down to the residual current values of 3 to 5 amperes. A plot of current as a function of electrolysis time is shown in Figure 10 for the electrolysis of $4LiF.CaF_2+Li_2O$(sat.) electrolyte. After completion of the electrolysis, alloy samples were withdrawn through an alumina tube and a rubber bulb attached to one end. The crucible was then removed from the furnace and the liquid alloy was poured into a nickel sample cup.

5.1.1 Chemical analysis of alloys for Lithium

0.5 gram samples of the alloy were dissolved in 1:1 concentration HCl and diluted to obtain solutions containing up to 2.5 ppm Li concentration. The solutions were analysed for lithium by atomic absorption spectrometry. At least 5 samples were analysed for each set of samples.

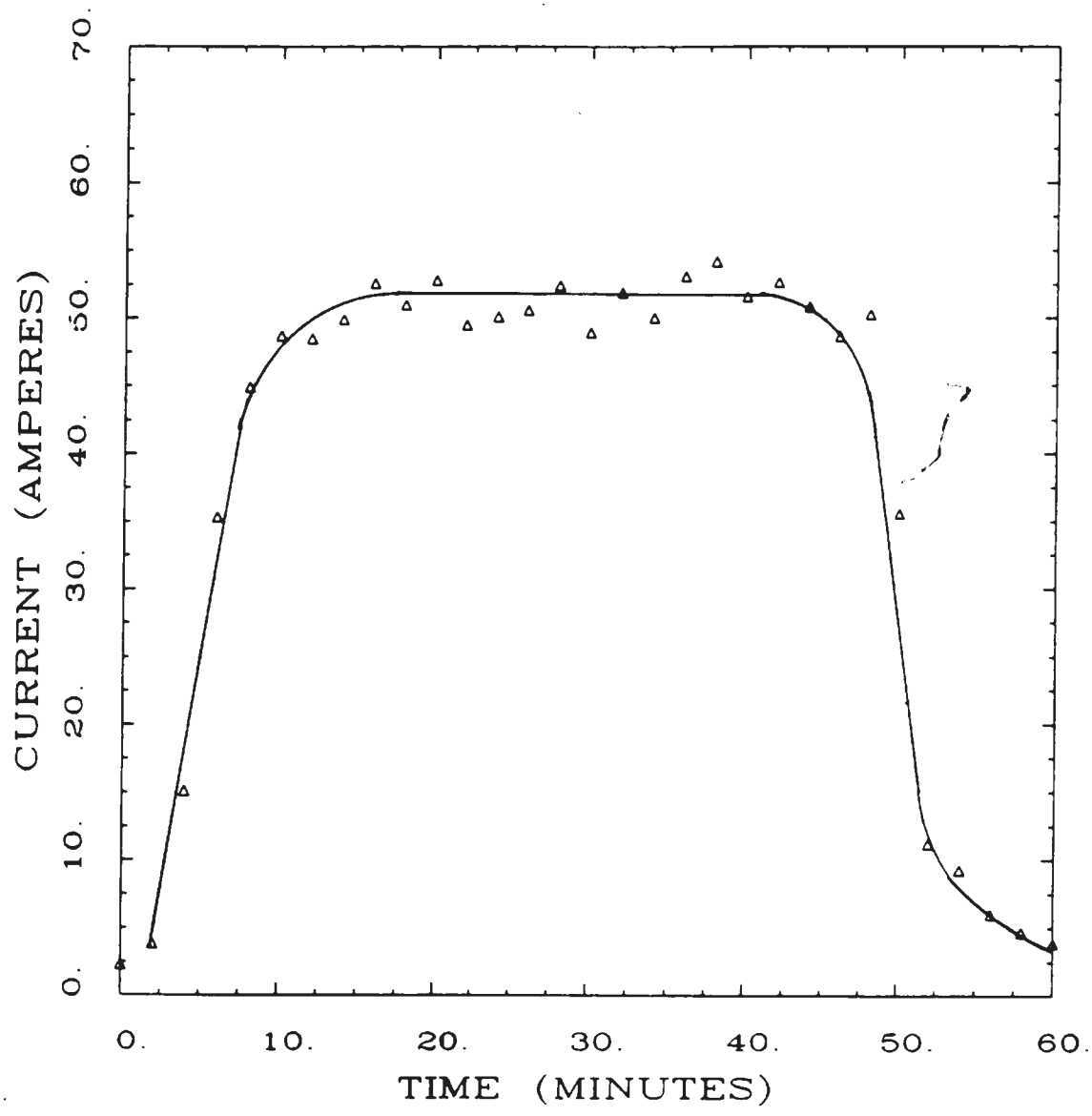

Fig. 10 Plot of current vs time for the electrolysis of $4LiF.CaF_2+Li_2O$(sat.) melt at 1121K

5.2 RESULTS AND DISCUSSION

The use of graphite anode results in a depolarization of the anode because of the reaction between oxygen and carbon to form CO_2. For the electrowinning of lithium overall cell reactions could be written:

$$2Li_2O(s) + C(s) = 4Li(l) + CO_2(g) \qquad (38)$$

The decomposition potential calculated from the free energy data (30) for the reaction 1 at 1073K is 1.355 volts. The difference in decomposition potentials of the fluorides and the oxide shown in Table 6 are sufficient to render the decomposition of the fluoride compounds unlikely.

At 1073K, the calculated density of the liquid Al-Li alloy (30 mole % Li) is 2.15 g/cm^3 (33) and that of liquid CaF_2-LiF electrolyte (79 mole % LiF) is 1.95 g/cm^3 (34,35). The density differences of 0.2 g/cm^3 should be sufficient for maintenance of a bottom liquid Li-Al cathode alloy and a top LiF-CaF_2 melt in the cell during electrolysis. For example, the Hall-Heroult aluminum cell operates with a density difference of 0.18 g/cm^3 between the bottom liquid aluminum cathode and the cryolite electrolyte (36).From the study of solubility of Li_2O in 4LiF.CaF_2 melts (section 3.2) between 1058 to 1133 K, the solubility of Li_2O was determined to be 10.1 to 14.8%. Hence for an electrolyte weight of 180 g, a weight of 30 to 32 g of Li_2O (16-17 wt.%) was found to be necessary to obtain a system saturated with Li_2O.

TABLE 6. DECOMPOSITION VOLTAGE FOR ELECTROLYTE AND CELL FEED COMPONENTS AT 1073K.

Compound	E°, volt
LiF	-5.3
CaF_2	-5.4
Li_2O	-2.3

While the liquidus temperature of composition $4LiF.CaF_2 + Li_2O$ was found to be 1004.5 $\pm$ 2.5K, it was difficult to run electrolysis below 1053 K because the melting point of the electrolyte increases with the depletion of Li_2O in the electrolyte and the viscosity of the melt is much higher within 20 K above the melting point of electrolyte (37). A summary of the results of the electrolysis experiments is presented in table 7.

5.2.1 Effect of Temperature

Effect of temperature on cathode current efficiency with a $4LiF.CaF_2 + Li_2O$ electrolyte is shown in Figure 11. All experiments were performed with an applied potential of 5 volts. As seen from the figure, the cathode current efficiency (K_{A-h}) increased with increase in temperature up to about 1121K and then decreased with further increase in temperature. The increase in efficiency may be due to the lower viscosity of the electrolyte. The viscosity (37) of the melt has a marked influence on the rate of diffusion of the Li^+ and O^{2-} ions to the respective electrodes. A possible reason for the reduction in cathode current efficiency at higher temperatures may be due to the back reactions where Li redissolves into the electrolyte. From the work done by Dworkin et al (38) on the phase equilibria of Li-LiF system, the solubility of Li in LiF is very low, below 1098K, as shown in Figure 12. However, a marked increase in solubility occurs above 1123K. Other alkali M-MF systems also showed similar behavior. Hence, it was found to be difficult to attempt to perform electrolysis experiments above 1123K in the present investigation.

TABLE 7. SUMMARY OF ELECTROLYSIS EXPERIMENTS

Temp. (K)	Electrolyte Composition	Cathode Current Efficiency (%)	Power Consumption KWH/lb Li	Recovery of Li (%)	Current Density (A/cm^2)	Average Current (A)
1155	$4LiF.CaF_2$ $+Li_2O$(sat.)	9.8	60.4	5.6	1.80	68.0
1136	"	18.1	43.3	6.7	1.27	49.0
1121	"	24.9	37.6	8.3	1.34	52.0
1099	"	21.7	43.1	10.5	2.19	58.0
1076	"	16.8	58.7	20.1	2.81	109.0
1057	"	15.5	61.8	6.9	1.70	38.0
1101	$5LiF.CaF_2$ (62.5 wt. % LiF)	26.8	31.8	11.9	2.37	63.0
1090	$7LiF.CaF_2$ (70 Wt. % LiF)	36.4	25.4	11.5	1.34	47.0
1133	pure LiF	43.0	23.7	13.4	1.10	42.0

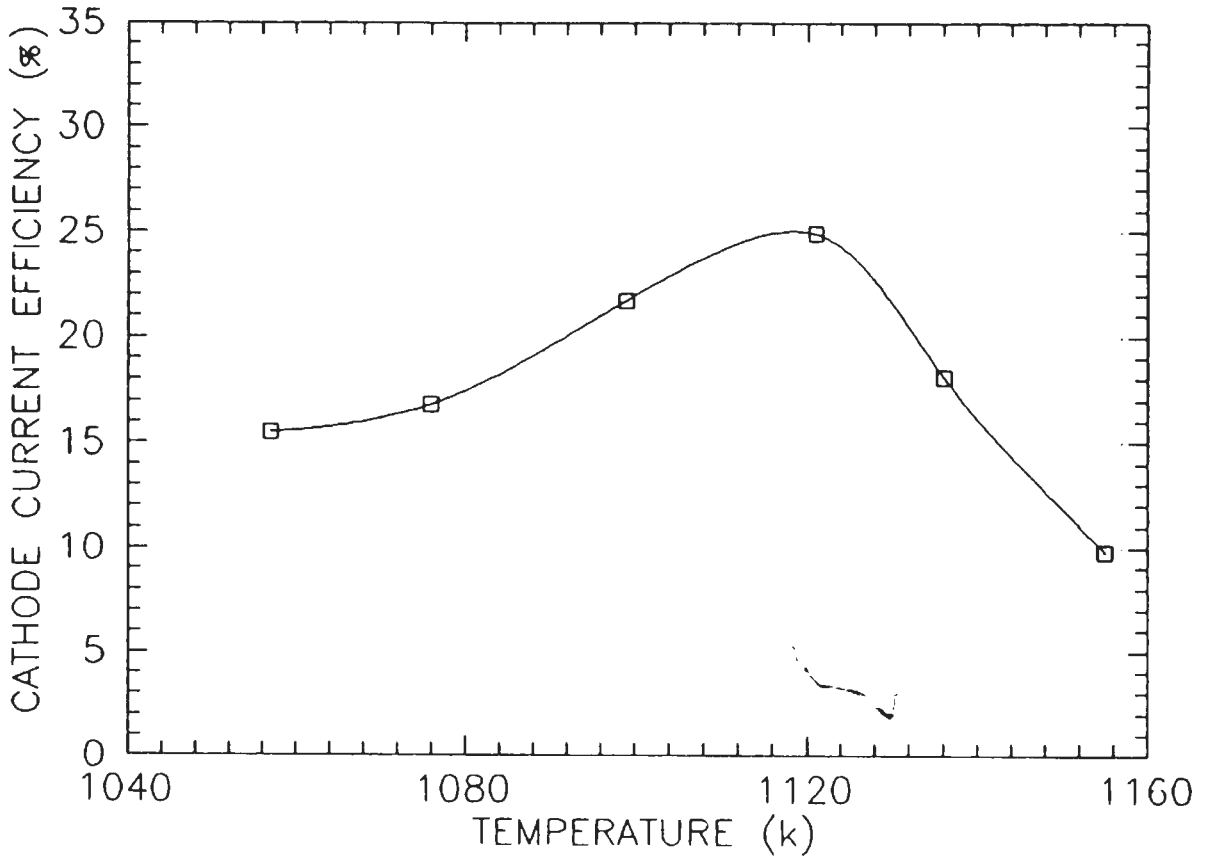

Fig 11. Effect of temperature on electrolysis of $4LiF.CaF_2 + Li_2O$(sat) electrolyte on cathode current efficiency between 1057 and 1155K

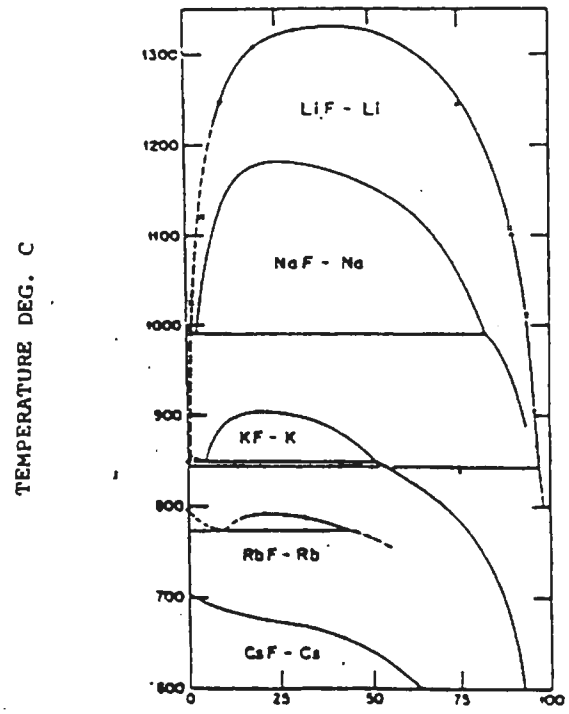

Fig. 12 Alkali metals-Fluorine systems

The power consumption as a function of temperature is shown in Figure 13. Similar to cathode current efficiency, the power consumption reached a minima with 37.6 KWH/lb at 1121K and increased with temperature above or below 1121K.

As seen from Figure 14, recovery of Li from Li_2O is the highest at a temperature of 1076K, 20.1%, and gradually decreased with increase in temperature. This behavior can again be explained by the lower solubility of Li in LiF at temperatures lower than 1093K.

5.2.2 Effect of Electrolyte Composition

The effect of electrolyte composition on the cathode current efficiency, recovery of Li and power consumption during the electrolysis was studied and results are presented in Figures 15, 16 and 17 respectively. All experiments were conducted in the temperature range of 1090 to 1101K, except the experiment with pure LiF which was carried out at 1133K.

As seen from Figure 15, the cathode current efficiency increased with increase in concentration of LiF in the electrolyte. For example, cathode current efficiency increased from 21.7% at 57.14 wt. % LiF to 43% at 100 wt. % LiF. However, the recovery of Li from Li_2O did not increase much with increase in LiF in the electrolyte as shown in Figure 16.

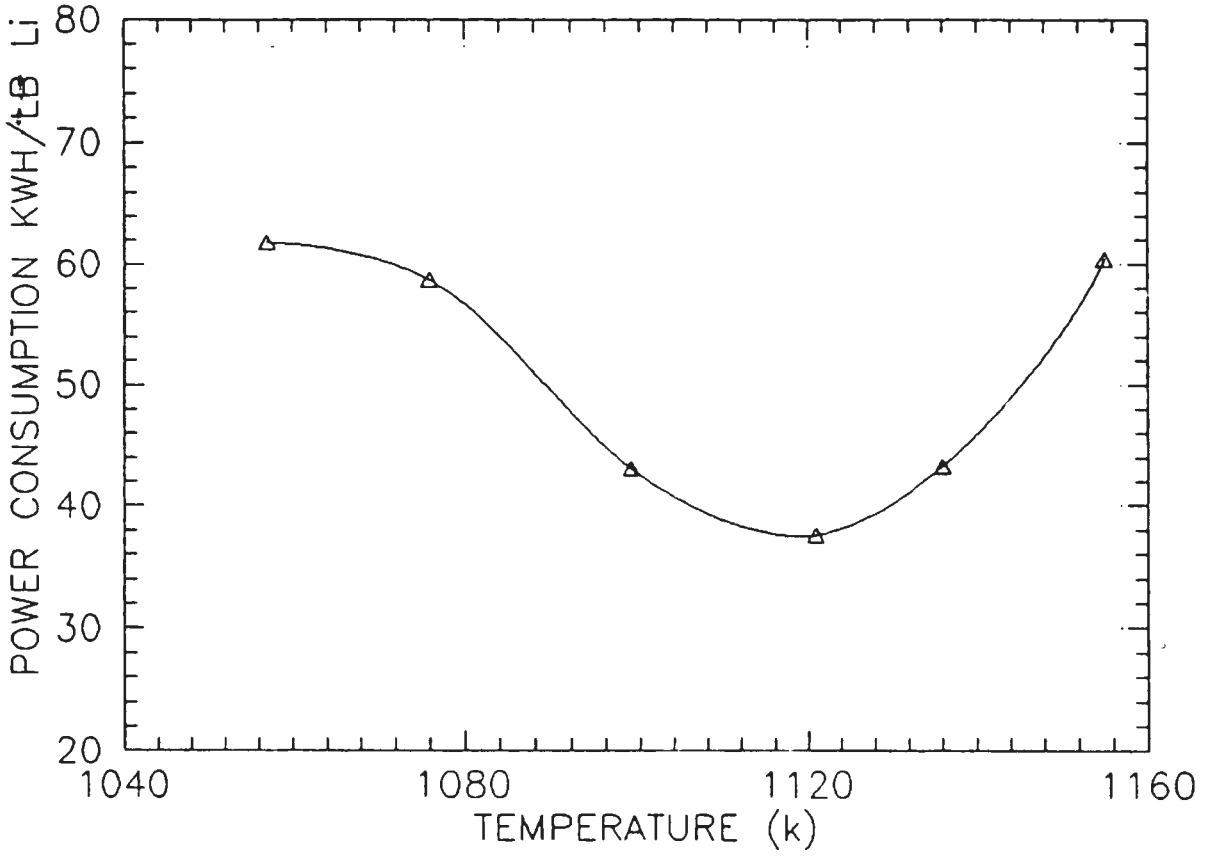

Fig 13. Effect of temperature of electrolysis of $4LiF.CaF_2+Li_2O$(sat.) electrolyte on power consumption between 1057 and 1155K

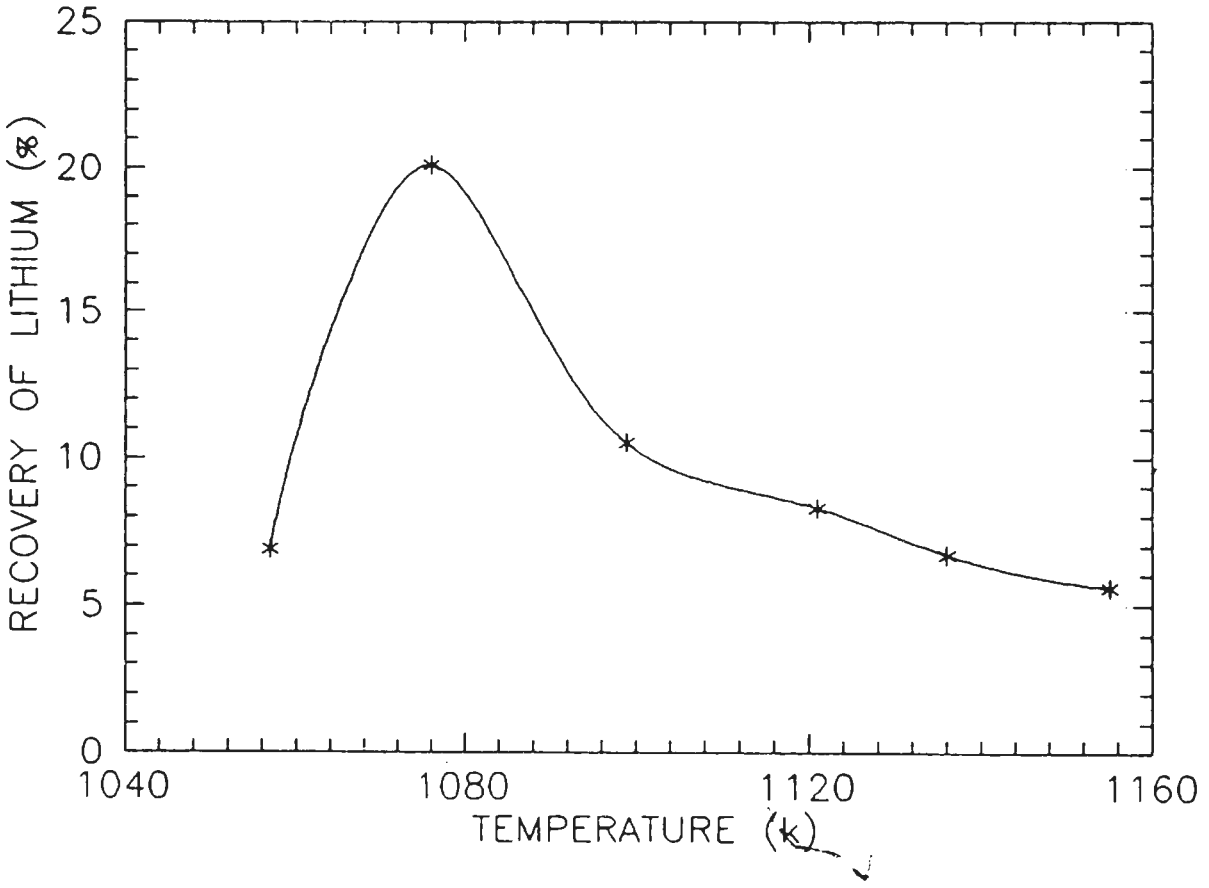

Fig 14. Effect of temperature of electrolysis of $4LiF.CaF_2 + Li_2O$ (sat.) electrolyte on recovery of Lithium between 1057 and 1155K

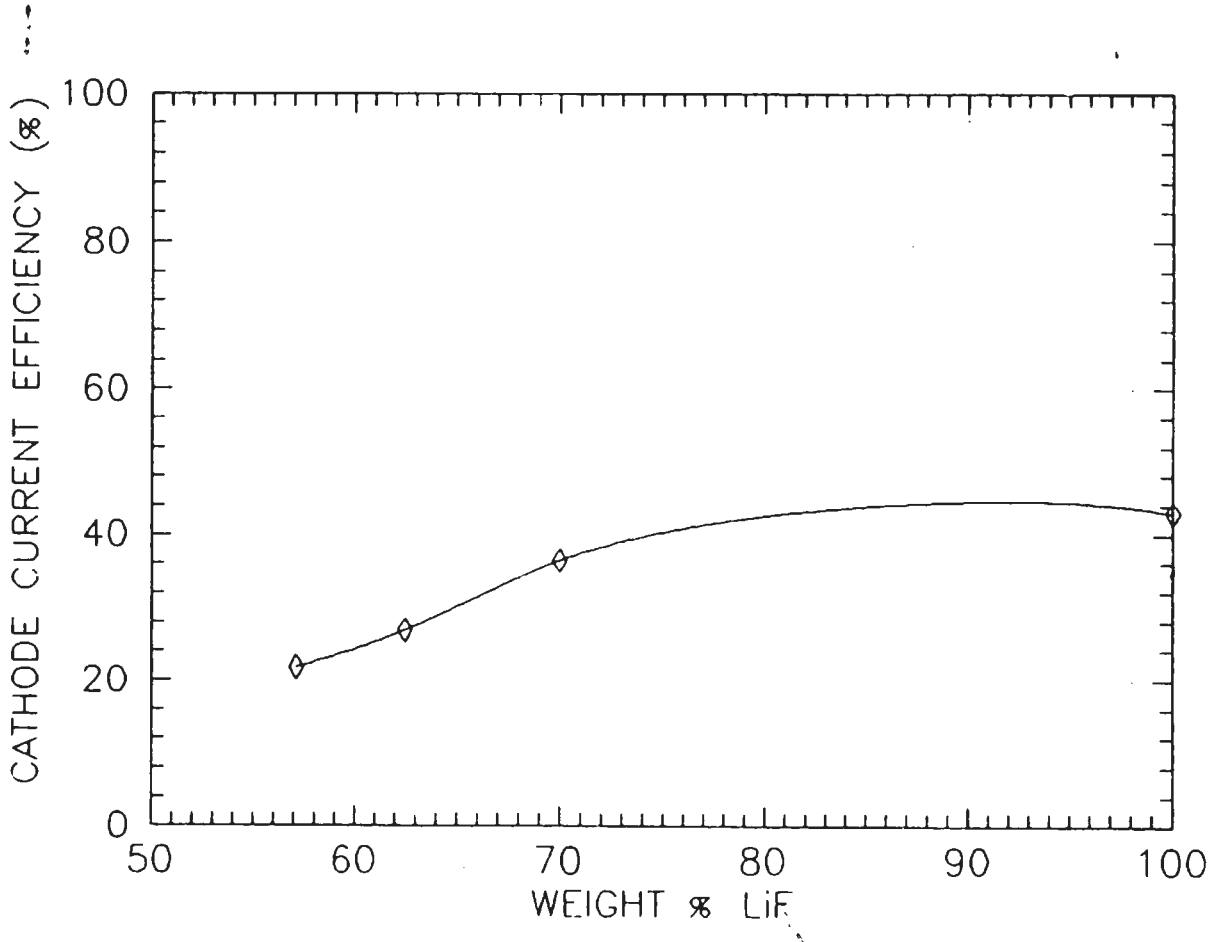

Fig 15. Effect of composition of electrolyte on cathode current efficiency in the temperature range of 1090 to 1101K except for pure LiF at 1133K

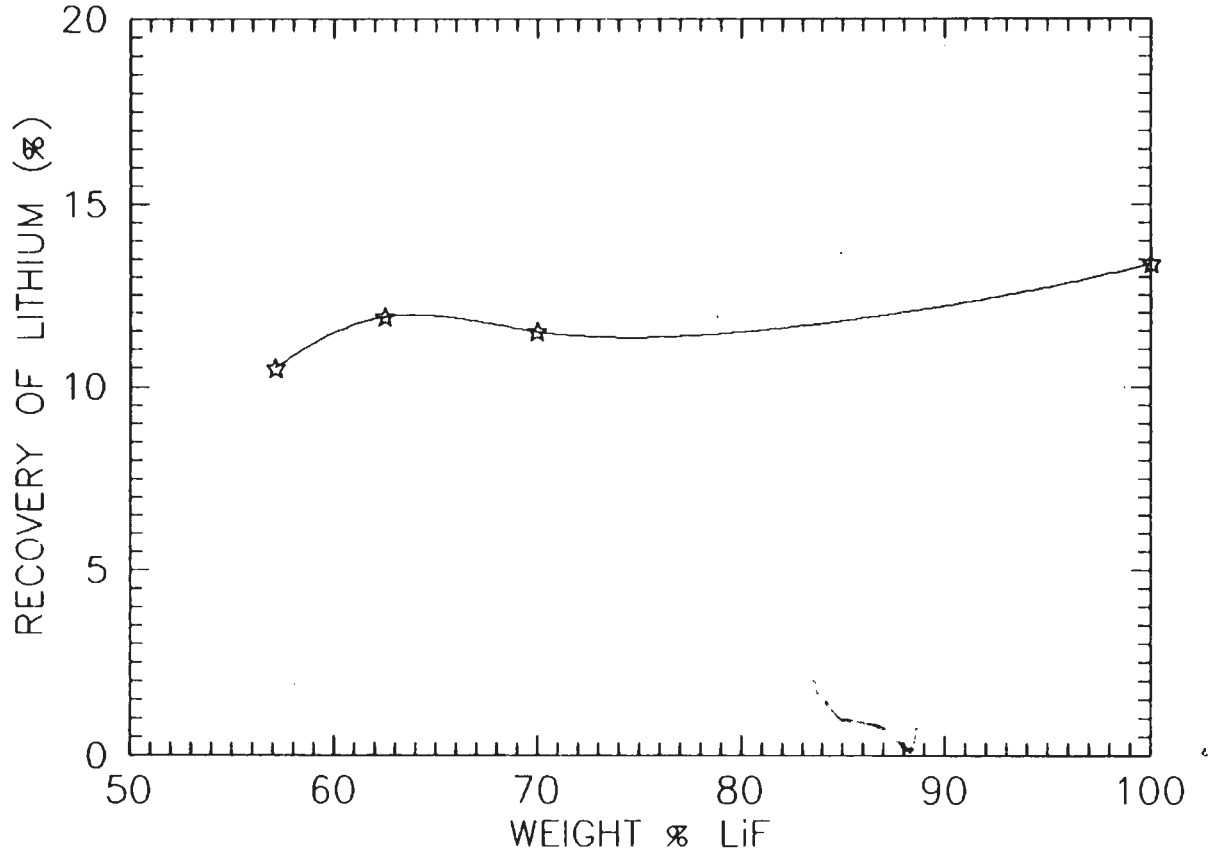

Fig 16. Effect of composition of electrolyte on recovery of Lithium in the temperature range of 1090K to 1101K except for pure LiF at 1133K

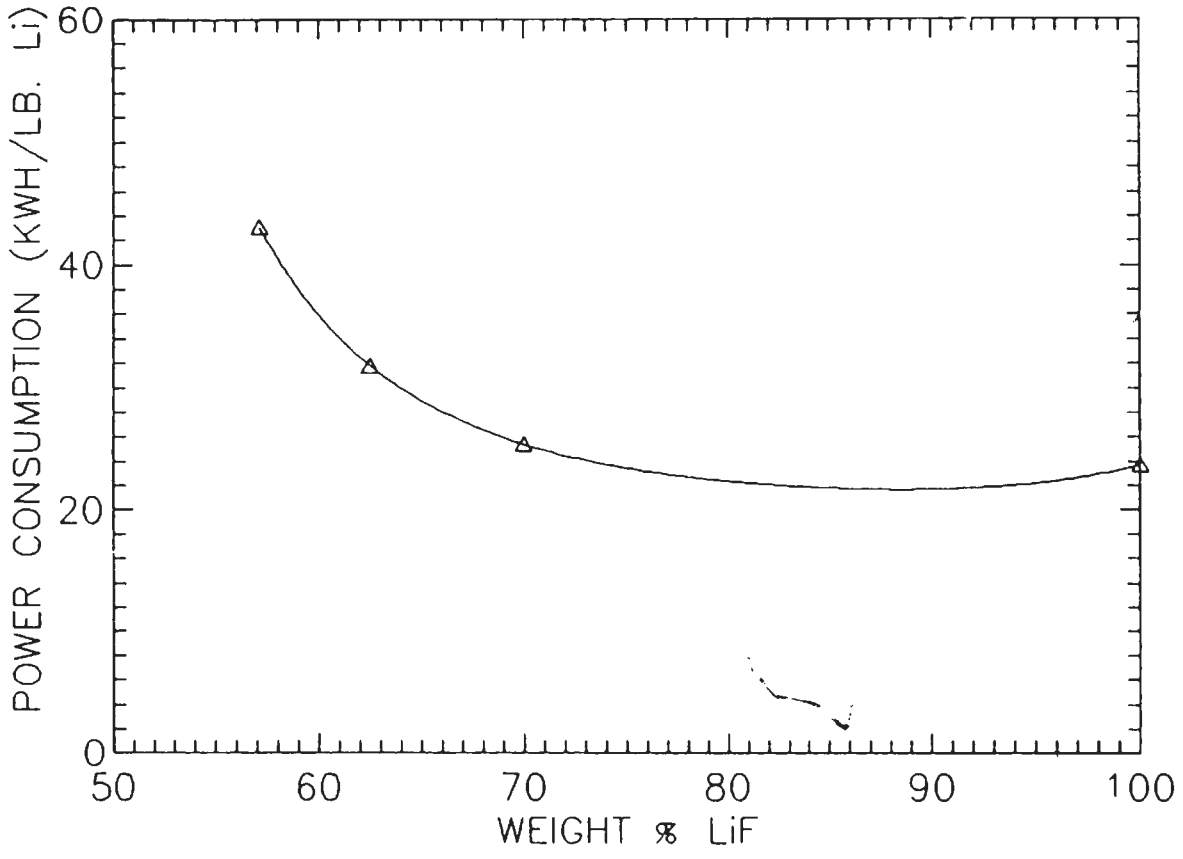

Fig 17. Effect of composition of electrolyte on power consumption in the temperature range of 1090K to 1101K except for pure LiF at 1133K

The maximum increase in recovery of Li, 13.4%, was observed with 100% LiF. As expected, the power consumption decreased with concentration of LiF in the electrolyte. A minimum value of power consumption, 23.7 KWH/lb, was obtained with 100% LiF in the electrolyte.

From the data obtained at various temperatures and melt compositons, it could be concluded that there is an optimum range of temperature (1073 to 1123K) at which an efficient electrolysis can be obtained. At low temperatures viscosity effects play an important role in reducing current efficiency while at higher temperatures redissolution of Li in electrolyte occurs. Melts with higher LiF work better with pure LiF giving the highest current efficiency.

6. SUMMARY

1. The solubility of Li_2O in 4LiF CaF_2 melts was found to increase from 10.6 wt.% at 1058 K to 14.8 wt. % at 1133K. The liquidus temperature of $4LiF.CaF_2$ + Li_2O(sat) melt was determined to be 1004.5 $\pm$ 2.5K. Activity coefficient of Li_2O in the melts as a function of temperature was deduced.

2. All anodic overvoltage vs log current density plots using a graphite anode, graphite reference electrode and $4LiF.CaF_2$ + Li_2O (sat) melt, showed a straight line relationship indicating a charge transfer controlled reaction. A value of η = 1.01 + 0.30 log i was obtained for the straight line region, with a Tafel slope of 0.30. A 2-electron controlled charge transfer reaction for the reaction between the complex oxyfluoride and the graphite anode was proposed and the complex species was predicted as $LiOF^{2-}$ and LiO_2F^{2-}. Limiting current density of 0.37 A/cm^2 in the melt was deduced. From the anodic polarization data, it was observed that a potential of at least 1.1 Volts is required in addition to the decomposition potential for electrolysis. From observations on the effect of stirring rate on the limiting current density, a limiting current phenomenon due to adsorption of CO on the anode surface was inferred.

3. Electrolysis of Li_2O in LiF-CaF_2 electrolyte was studied as a function of temperature and composition using a liquid Al cathode and graphite anode. The mean cathode current efficiency showed a

value of 24.8% at 1121K and the power consumption showed a minimum of 37.6 KWH/lb of lithium. Higher viscosity of the melt at lower temperatures and redissolution of Li at higher temperatures gave lower values for cathode current efficiency. The cathode current efficiency increased with increasing wt. % of LiF in the electrolyte and the power consumption showed a reverse trend. Higher cathode current efficiency (43%) and lower power consumption of 23.7 KWH/lb was obtained with pure $LiF+Li_2O$(sat.) as electrolyte at 1133K.

4. An optimum cathode current efficiency of 24% at 1121K with $4LiF.CaF_2+Li_2O$(sat.) electrolyte and 36% with $7LiF.CaF_2+Li_2O$(sat.) electrolyte was obtained. The cell efficiency can be improved by reducing liquidus temperature of the electrolyte. Further studies on the effect of fluoride additions to form low melting electrolytes is recommended. Finally, it must be mentioned that the above process offers a viable alternative to the existing methods of producing aluminum lithium alloys and measures to optimise the process parameters would go a long way in improving the cell efficiency.

REFERENCES

1. Quist, W. E., Narayanan, G. H. and Wingert, A. L., Aluminum-Lithium Alloys-II, ed. T. H. Sanders Jr. and E. A. Starke Jr., TMS-AIME, 1983, p. 313.

2. Starke, E. A. Jr. and Sanders, T. H., J. of Metals, vol.8,August, 1981, p. 24.

3. Verma, R., Argonne National Laboratories, private communication, 1986.

4. Fulmer Research Institute (England)., "Low Density, High Strength, Al-Mg Alloys Containing Lithium" undated advertising flyer.

5. Chemical Marketing Reporter,1987.

6. Siraev, N.S., Tsvetn. Met., vol. 10,October, 1982 , p. 36. (Russian)

7. Belov, S. F. and Gladeneva, A.F., Izv. V.U.Z. Tsvetn. Met. vol.4,1982 , p. 83. (Russian)

8. Belov, S. F. and Gladeneva, A.F., Sov. NonFerrous Met. Res. ,vol. 4,1981 , p. 2673.

9. Belov, S. F. and Gladeneva, A.F., Sov. NonFerrous Met. Res. ,vol. 4,1981, p. 480.

10. Belyayaev, A.I., Metallurgy of Aluminum, V.E.B. Verlag Technik, vol. 1, 1957,p.103.

11. Stern, K. H., presented at 18th I.U.P.A.C. Conference, Montreal, August 1961.

12. Haupin, W. E., Light Metals, 1979, p. 45.

13. Wai, C. M. and Blander, M., Z. Naturforsch, vol. 39a,1984, p.499.

14. Suito, H. and Gaskell, D. R., Met. Trans. B., Vol. 7B, Dec. 1976, p. 567.

15. Guanxian Xu and Jimei Xiao., "Proceedings of International Conference on Rare earth developments and applications", Beijing, People's Republic ofChina,Sept. 10-14,1985, Academic Press,1986.

16. Morrice, E., Shedd, E. S. and Henrie, T. A., U.S.B.M. Report of Investigation No. 7146, 1968.

17. Morrice, E. M. and Henrie, T. A., U.S.B.M Report of Investigation No. 5549, 1960.

18. Porter, E. and Brown, E.A., U.S.B.M Report of Investigation No.

5878, 1961.

19. Bratland, D. and Grojtheim, K., Revue Roum. Chim. Vol.17, 1-2, 1972, p.41.

20. Boe, G., Ph.D. thesis, Univ. of Trondheim, Norway, 1976.

21. Bratland, D., Boe, G. and Grojtheim, K., Revue Chim. Miner. vol. 10, 1973, p. 347.

22. Aamland, E.,Macdonald, D. J. and Kesterke,D. G., U.S.B.M. Report of Investigation No. 6226, 1963.

23. Butorov, V. P. and Novikov, E.A., Tr. Ural. Politech. Inst. vol. 220, 1973, p. 77-81. (Russian)

24. Saboungi, M.L. and Hsu, C.C., CALPHAD, Vol. 1(3), 1977, p. 237.

25. Myles, K. M., Mrazek, F. C., Smaga, J. A. and Settle, J. L., Proceedings of the Symposium and Workshop on Advanced Battery Research and Design, U.S. ERDA Report, ANL 76-78, 1976, p. 8-50.

26. Hansen, D. A. and Smith, J. F., Acta Cryst., B., Vol. 29, 1968, p. 913.

27. Roake, W. E., J. Electrochem. Soc., Vol. 104, 1957, p. 661.

28. Palmer, T.A., Talanta, vol. 19,1971, p.1141, Pergamon Press.

29. Suiter, D. J., Report MDC E 26788, U.C-20, June 1983.

30. Stull, D. R. and Prophet, H., "JANAF Thermochemical Tables," NSRDS-NBS 37, U.S. Dept. Commer., Washington, DC, 1971.

31. Vetter, K. J., Electrochemical Kinetics, Academic Press, NY, 1967.

32. Thornstad, J., Electrom. Acta, Vol. 15, 1970, p. 1569.

33. Edwards, J. D. and Moorman, T. A., Chem. Met. Eng., Vol. 24, 1921,p.61.

34. Jeager, F. M. A., Anorg. U. Allgem. Chem., Vol. 101, 1917, p. 177.

35. Keene, B. J. and Mills, K. C., The Physical and Chemical Properties of Slags, NPL Report, Chem. 60, London, Nov. 1976.

36. Mantell, C. L., Electrochemical Engineering, McGraw Hill, New York, 1960, p. 385.

37. Molten Salts Handbook, ed. by Janz, G.J, Academic Press, New York, 1967,p. 39-52.

38. Dworkin, A. S., Bronstein, H. R. and Bredig, M. A., J. Amer. Chem. Soc., vol. 66, 1962, p.572.

APPENDIX

1. Error Estimation

The total error involved in the estimation of liquidus composition of Li_2O is as follows:

$$E_T\ (\%) = E_{Ca}\ (\%) + E_{Li}\ (\%) + E_F\ (\%) + E_O(\%)$$

In the analysis of Ca and Li by atomic absorption spectrometry,

$$E_{Ca}\ (\%) = \pm\ 0.64$$

$$E_{Li}\ (\%) = \pm\ 0.44$$

In the analysis of F by the ion selective electrode method,

$$E_F\ (\%) = \pm\ 0.5$$

In the analysis of O by the inert gas fusion technique,

$$E_O\ (\%) = \pm\ 0.5\%$$

Total maximum error = $\pm$ 2.18%

2. Calculation of cell efficiency

In section 4. the following cell parameters were used in determining the efficiency of the cell.

a. Cathode current efficiency

The cathode current efficiency (C.C.E. in %) is expressed as the ratio of the theoretical ampere hours required to deposit lithium to the actual ampere hours consumed to deposit the same quantity of metal. At 100% efficiency, it requires 3.828 ampere hours to deposit one gram of lithium.

b. Energy consumption

This quantity in kilowatt hours per pound can be defined as the actual energy required to deposit one pound of lithium in the aluminum.

c. Recovery of lithium

This quantity is expressed as the ratio of actual weight of lithium deposited to weight of lithium added in the form of lithium oxide.

A detailed calculation of the cell efficiency is provided below for the electrolysis of $4LiF.CaF_2 + Li_2O$ (sat) electrolyte at 1076K.

Data

weight of electrolyte = 187.1 g

weight of aluminum = 150.0 g

weight of lithium oxide = 35.8 g

weight of alloy recovered = 139.2 g

time of electrolysis = 78 minutes

surface area of anode in contact with electrolyte = 38.73 cm^2

average voltage = 5.14 volts

average current = 109 amperes

total ampere hours consumed = 77.08

total power consumed = 437 watt hours

The total ampere hours and total power (watt hours) were calculated from measurements of current and voltage at an interval of 2 minutes.

A total of 5 samples were analysed for lithium content with an average of 2.43 weight % of lithium

average weight of lithium deposited = 3.382 g

It would require 12.946 ampere hours to deposit 3.382 grams of lithium at 100% cathode current efficiency, hence the average cathode current efficiency (%)

$$= \frac{12.946}{77.08} \times 100\% = 16.8\%$$

It required 437 watt hours to deposit 3.382 grams of lithium.

Hence power consumed per pound of lithium deposited

$$= \frac{0.437}{3.382} \times 454 = 58.66 \text{ KWH/lb}$$

A quantity of 3.382 grams of lithium was recovered from 35.8 grams of lithium oxide.

$$\text{Hence recovery of lithium} = \frac{3.38 \times 100}{35.8 \times 0.4666}$$

$$= 20.24\ \%$$